An experimental and kinetic modeling study of benzene pyrolysis with C2–C3 unsaturated hydrocarbons

Alaa Hamadi, Wenyu Sun, Said Abid, Nabiha Chaumeix, Andrea Comandini

Combustion and Flame 237 (2022) 111858

Contents lists available at ScienceDirect

Combustion and Flame

journal homepage: www.elsevier.com/locate/combustflame

An experimental and kinetic modeling study of benzene pyrolysis with C2−C3 unsaturated hydrocarbons

Alaa Hamadi[a,*], Wenyu Sun[a], Said Abid[a,b], Nabiha Chaumeix[a], Andrea Comandini[a,*]

[a] CNRS-INSIS, I.C.A.R.E., 1C, Avenue de la recherche scientifique, 45071 Orléans cedex 2, France
[b] Université d'Orléans, 6 Avenue du Parc Floral, 45100 Orléans, France

ARTICLE INFO

Article history:
Received 8 July 2021
Revised 3 November 2021
Accepted 4 November 2021

Keywords:
Benzene
Acetylene
Ethylene
Propylene
Propyne
Polyaromatic hydrocarbons (PAHS)
Soot formation
Single-pulse shock tube

ABSTRACT

A combined experimental and kinetic modeling study is carried out to explore the influences of added acetylene, ethylene, propylene, and propyne on the reaction schemes of benzene pyrolysis. Pyrolysis of benzene with and without the presence of the C_2- or C_3- unsaturated hydrocarbons (HCs) is conducted in a single pulse shock tube coupled to gas chromatography-mass spectrometry technique. A minimum of 30 species is detected in each reaction system, and their mole fraction profiles are obtained over the temperature range 1030–1800 K at a nominal pressure of 20 bar and a nominal reaction time of 4 ms. With updates based on recent theoretical studies, our ongoing detailed kinetic model with 552 species and 4958 reactions can successfully reproduce the decomposition reactivity of the fuels, formation of decomposition products, and the growth of aromatics in the pyrolysis of different fuel mixtures. Various considerations apply to all studied binary mixtures. The addition of C_2- and C_3- HCs to the reaction system leads to C_2H_2 formation, and consequently promotes the HACA mechanism starting from phenyl radical (C_6H_5) at relatively low temperatures. The resulted phenylacetylene, formed through $C_6H_5+C_2H_2$ reaction, promotes the addition-elimination reaction $C_6H_5C_2H + C_6H_5$ leading to the enhanced and early formation of all $C_{14}H_{10}$ PAH isomers including ethynyl biphenyl, methylene-fluorene, diphenylacetylene, phenanthrene, and anthracene. It is also noteworthy that the existence of C_2H_2 as fuel or its production from C_2H_4, C_3H_6, and C_3H_4-P decomposition results in numerous compounds with ethynyl branches such as ethynyl biphenyl, diethynyl naphthalene, and ethynyl acenaphthylene. Considering the specific features of the different fuel mixtures, the addition of acetylene intensifies the HACA route leading to greater acenaphthylene formation, while naphthalene formation remains similar to the pure benzene case due to the limited H-atoms. Differently, in benzene-C_2H_4 co-pyrolysis, naphthalene and acenaphthylene are mainly formed through reactions between PAH radicals (phenylacetylene radical and naphthyl radical, respectively) and ethylene. Concerning benzene-C_3 co-pyrolysis, indene is the major C_9 species resulting from the reaction of benzene/phenyl with C_3 fuels. This is an important theoretical pathway to indene which is experimentally probed here for the first time. The high concentration of indene leads to the enhanced formation of naphthalene and acenaphthylene through the reactions of indenyl radical with methyl and propargyl (C_3H_3) radicals, respectively. Afterwards, the naphthyl radicals participate in the formation of several larger C11–13 PAHs such as methylnaphthalene, ethynylnaphthalene and fluorene through their reactions with CH_3, C_2H_2 and C_3H_4-P/C_3H_3, respectively.

1. Introduction

The detailed understanding of soot formation in modern combustion devices is one of the most challenging topics in the chemical kinetics field. In particular, the complex processes leading to the first particles, including the formation and growth of the polycyclic aromatic hydrocarbon (PAH) precursors, need to be fully explored in order to be able to develop accurate chemical kinetics models for soot particle emissions. Nowadays, the investigations on PAH chemistry are rather sparse due to the large number of possible reaction pathways, the limitations in the experimental techniques as well as in the theoretical methods [1]. Pyrolytic studies on simple reactants and mixtures can be used to isolate the PAH formation and growth processes from the oxidation steps,

* Corresponding authors.
E-mail addresses: alaa.hamadi@cnrs-orleans.fr (A. Hamadi), andrea.comandini@cnrs-orleans.fr (A. Comandini).

https://doi.org/10.1016/j.combustflame.2021.111858

Table 1
Literature studies on benzene pyrolysis.

Literature	Facility	Conditions	Model	Objective
Hou et al. [6], 1965	tubular flow reactor	1% C_6H_6 in He, T = 1173–1523 K, p = ~735 torr, τ^*= 20–250 ms	No model	speciation + rate constants calculation
Kern et al. [7]., 1982	Shock tube/ time-of-flight mass spectrometer	T = 1415–2190 K, p = 0.21–0.57 atm, τ= 700–1000 µsec	No model	speciation
Laskin and Lifshit [8], 1996	Shock tube/ gas chromatography	0.3% C_6H_6 in Ar, T = 1400–2000 K, p = ~5 atm, τ= 2 ms	15 species, 22 reactions	speciation + model development
Sivaramakrishnan et al. [9]., 2006	Shock tube/ gas chromatography	0.0063%, 0.0084% 0.08% C_6H_6 in Ar, T = 1200–1800 K, p = 30 - 50 bar, τ= 1.2–1.5 ms	98 species, 544 reactions	speciation + model development
Tranter et al. [10], 2010	Shock tube/ time-of-flight mass spectrometry and laser schlieren	2% C_6H_5I in Ne, T = 1276–1853 K, p = 25, 54,122, and 500–700 Torr, τ= 250 µsec	21 species, 30 reactions	speciation + model development and theoretical calculation
Bohm et al. [11]., 1998	Shock tube/ He–Ne laser	T = 1600–2400 K, p = 60 bar, τ= 20–250 ms	Number of reactions and species not mentioned	speciation + model development
Shukla and Koshi [12], 2010	Flow tube Reactor/ vacuum ultraviolet single photon ionization time of flight mass spectrometry	40% C_6H_6 in He and 20% C_6H_6 + 20% C_2H_2 in He T = 1140–1473 K, p = 10.18 Torr, τ= 0.61 s	–	kinetic analyses
Comandini et al. [13], 2012	Shock tube/ gas chromatography	0.0025%, 0.005%, 0.01% C_6H_5I in Ar, 0.005% C_6H_6 + 0.025–0.05% C_2H_2 in Ar T = 900–1800 K, p = 25 and 50 atm, τ=1.5–2 ms	112 species, 309 reactions	speciation + model development
Saggese et al. [14], 2013	–	–	350 species, 1000 reactions	kinetic model validation for benzene pyrolysis and oxidation
Sun et al. [15], 2021	Shock tube/ gas chromatography	0.02% C_6H_6 in Ar and T = 1100–1800 K, p = 20 bar, τ= 4 ms	203 species, 3428 reactions	speciation + model development

$^*\tau$ is the reaction time in shock tube experiments and residence time in flow reactor experiments.

reducing the complexity of the kinetic problem and helping the understanding of the fundamental processes responsible for soot formation.

Among the aromatic intermediates whose chemistry strongly affects the soot kinetics, benzene (C_6H_6) is a minor component of conventional fuels [2,3], but a relevant intermediate of several combustion processes. In particular, it is considered as a fundamental building block for polycyclic aromatic hydrocarbons (PAHs) and soot growth [4,5]. Given its central role, several kinetic studies have investigated the C_6H_6 thermal decomposition [6–10] and the related PAH formation chemistry [11–15], as summarized in Table 1. These studies include investigations on the phenyl radical (C_6H_5) pyrolysis, the main product from the initial thermal decomposition steps of benzene. Besides dissociation and self-recombination [10,16–19], phenyl reacts with other species present in the reaction system contributing to PAH growth. The interaction between aromatic fuels and the typical small unsaturated hydrocarbons present in all combustion environments represents fundamental pathways for the PAH growth. Thus, an accurate description of the relevant reaction mechanisms is needed for the development of reliable and robust combustion kinetic models. These models are highly required for numerical simulations that are used in developing high-performance clean combustion technologies.

Reactions of C_6H_6/C_6H_5 with C_2-C_3 unsaturated hydrocarbons, which are usually abundant in combustion reaction systems, can potentially lead to ring growth. To address the effects of C_2H_x/C_3H_x addition on phenyl radical, various experimental and theoretical studies were carried out, some of which derived rate coefficients of the relevant reactions [16,20–33]. Benzene pyrolysis especially with the presence of acetylene (C_2H_2), ethylene (C_2H_4), propene (C_3H_6) or propyne (C_3H_4-P), can provide ideal environments to inspect these reaction channels. To the best of our knowledge, the essential interactions between C_6H_6 and C_3H_4-P/C_3H_6, which can lead to the formation of indene, have never been directly examined through experimental methods. Besides, although the hydrogen-abstraction-acetylene-addition (HACA) mechanism has been established as a vital pathway of PAH formation and growth [20,34,35], there are only few experimental studies on the pyrolysis of benzene-C_2H_2, which is highly relevant to the HACA route from benzene to naphthyl. Shukla and Koshi [12] analyzed the highly efficient mechanisms of PAHs growth for the pyrolysis of benzene with and without addition of acetylene and for pure acetylene. The pyrolytic reactions were obtained in a flow reactor coupled to a vacuum ultraviolet (VUV) single photon ionization (SPI) time of flight mass spectrometry (TOFMS) at a constant pressure of 10 Torr. The authors remarked that the only difference between pure benzene and benzene + acetylene mixture is the higher production of phenylacetylene and phenanthrene at low temperatures, while no significant influence of acetylene addition to benzene was observed at high temperatures. Later, Comandini et al. [13] carried out phenyl iodide and phenyl iodide + acetylene pyrolysis experiments using a high pressure shock tube (HPST)

at nominal pressures of 25 and 50 atm for a temperature range between 900 and 1800 K. A kinetic model was developed based on the experimental results, in particular focusing on the PAH formation mechanisms. The above-mentioned flow reactor pyrolysis experiments were performed at sub-atmospheric pressure, while the shock tube pyrolysis experiments were conducted using phenyl iodide as a precursor of phenyl. Hence, it is still necessary to analyze the role of the proposed PAH formation pathways via direct benzene-acetylene pyrolysis experiments at conditions relevant to practical combustion operations. Despite the fact that Shukla and Koshi [36] postulated that the PAH growth initiated by hydrogen abstraction and vinyl radical addition (HAVA) is more efficient than the HACA route, how C_2H_4 reacts with benzene and its influence on the PAH speciation at engine-like conditions received relatively less attention. In particular, the HAVA mechanism was observed at low pressures (20 Torr) where the vinyl radical can survive long enough to contribute to the PAH growth. At the typical high-temperature high-pressure combustion conditions, C_2H_3 decomposition may be too fast to allow the HAVA route to be effective even when the precursor ethylene is present in the initial mixture. On the other hand, our recent works [37,38] showed that C_2H_4 and C_2H_2 have different impacts on the PAH formation, especially regarding naphthalene and acenaphthylene in phenylacetylene pyrolysis [37] and indene in toluene pyrolysis [38].

Based on the brief review presented above, it is clear how a comprehensive and detailed study on the interaction between benzene and C_2/C_3 unsaturated hydrocarbons could provide new insights on some of the fundamental pathways to soot precursor molecules which haven't been addressed yet. Consequently, the present article focuses on two major topics: i) providing reliable shock tube pyrolysis datasets for the different benzene + C_2/C_3 mixtures at practical conditions (~20 bar, 1050−1770 K); ii) comparing the effects of adding C_2H_2, C_2H_4, C_3H_6 and C_3H_4-P to benzene pyrolysis, in relation to the fuel decomposition reactivity and PAH formation pathways. Intermediate species, including PAHs up to three-rings, are quantified using the gas-chromatography and mass spectrometry techniques. The comprehensive and detailed concentration measurements are used to facilitate the development of our on-going PAH kinetic model in serial works [15,38–40]. Updates are made based on recent theoretical results and the updated model is validated against the current experimental data. Modeling analyses are performed to gain insights into the chemistry of fuel decomposition and aromatic growth in benzene-C_2/C_3 pyrolysis.

2. Shock tube pyrolysis experiments

The experimental work is carried out with the high-purity single-pulse shock tube facility at ICARE-CNRS, Orleans, France. The single-pulse shock tube apparatus consists of the driven (length: 6 m; inner diameter: 78 mm) -and the driver (length: 3.7 m; inner diameter: 120 mm) sections, separated by a double diaphragm. A dump tank of 150 L volume is placed close to the diaphragm on the driven section side in order to operate the shock tube in the single-pulse fashion. The various parts composing the shock tube are made of 304 L stainless steel. The low-pressure section is heated to 90 °C to avoid the condensation and the absorption of fuels and heavy reaction products. To avoid carbon deposits, the inner shock tube surface is cleaned regularly. For further details on the shock tube setup, see earlier studies [15,37–40].

Four pressure sensors (CHIMIE METAL A25L05B) coupled to fast digital oscilloscopes (Tektronix model TDS5034B and Keysight Technologies model DSOX2014A) are mounted with a distance interval of 150 mm along the ending part of the driven section, with the last one being 82 mm away from the end wall. The time taken for the shock wave to pass each interval is used to derive the velocity of the incident wave. This value together with the initial pressure, temperature, and mixture composition (test gas) allow the determination of the temperature and pressure behind the incident and the reflected (T_5 and p_5) shock waves by solving the conservation equations [41–43]. This method has been proven to give accurate thermodynamic conditions behind the reflected shock waves for defined shock wave speeds and initial conditions. For each experiment the time-history pressure profile is also provided for accurate simulation of the results. A different method to derive T_5 in single-pulse shock tube experiments adopted by various research groups involves the use of chemical thermometers to derive averaged temperatures throughout the entire reaction process [44]. Such method compensates for the non-idealities encountered in the experimental measurement, but it is subject to certain uncertainties related to: i) the measurement of the incident shock wave velocity; ii) the definition of the unimolecular reaction rate constant parameters for the selected species; iii) extrapolation of the calibration curves outside the temperature range of the chemical thermometers (valid mainly for temperatures higher than 1350–1400 K). In addition, previous studies have shown how the use of chemical thermometers [45,46] or constant pressure conditions [15,37–40] cannot correctly account for the reactions involving the resonantly-stabilized radicals. Considering that the present work is performed with a shock tube of large bore where the non-idealities are minimized, the current method based on the theoretical T_5 calculation is preferred here. The maximum estimated uncertainty of the calculated T_5 is around ±30 K. This estimate is based on considerations related to the physical dimensions of the sensors (2 mm in diameter, 1.2 mm sensitive area) which may cause an error in the correspondence between the signal rise due to the passage of the wave and the actual position on the sensitive surface. This is a conservative estimate which includes also the uncertainties due to the attenuation of the wave. A PCB Piezotronics pressure sensor, shielded by a layer of room-temperature vulcanizing (RTV) silicone, is mounted on the end wall of the driven section and is used to record the pressure history for each shock from which the corresponding reaction time can be defined [47]. The reaction time is the time interval between the arrival of the shock wave and time when the pressure drops to 80% of p_5 (a typical pressure profile with the reaction time is shown in **Fig.S1**). The nominal reaction time in the current experimental configuration is 4 ms. The post-shock mixtures are sampled by an air-actuated valve, supplied by the High Pressure Equipment Company (HiP model 30–11HF4), fixed at the center of the end wall. The sampling valve is triggered by the end wall pressure sensor with a delay of 4 ms which is equivalent to the nominal reaction time. The opening and the closing of the valve requires hundreds of milliseconds, resulting in a relatively large sample volume which makes very small concentrations of PAHs ($\sim 10^{-2}$ ppm) detectable. Because of this large sample volume, the average velocity is used instead of the extrapolated one for T_5 and p_5 determination as it resembles more the real conditions encountered by the fuel mixtures. The velocity attenuation for the most experiments is below 2.5%, so the difference between the T_5s calculated with the average velocity and the extrapolated ones is generally lower than 20 K, which is within the uncertainty mentioned above. It is also noteworthy that the long sampling time does not affect the species concentrations due the very low temperature at the end of the quenching period.

The withdrawn post-shock samples are transferred to the analytical system through SilcoTek lines heated to 210 °C to prevent any condensation. An Agilent GC, series 7890B, is placed in series with a Thermo Trace GC Ultra coupled to a Thermo DSQ mass spectrometer (MS). The first GC, designed particularly to measure the PAHs up to four rings, is equipped with a flame ionization detector (FID) coupled to a DB-17 ms column for heavy species

separation, and a thermal conductivity detector (TCD) coupled to a Molseive 5A column for monitoring the absence of air and the dilution level from the helium driver gas. An external valve box capable to regulate the temperature up to 320 °C is used for this GC to minimize the loss of heavy compounds resulting from condensation during storage. The second GC is equipped with an FID detector connected to an HP Plot Q column for measuring light species up to mono-aromatic species. A DSQ mass spectrometer is also connected to aid species identification based on the ionization fragmentation patterns. For this purpose, the Thermo GC/MS is equipped with the same column as that for the FID of the Agilent GC in order to have similar retention times for the PAH compounds and thus easier comparison between the different analyses.

The identification of PAH species is confirmed through a combination of the known retention times from prior PAH standards' injections and the mass spectra. The quantification of the measured species relies on calibrations for the FID responses which are conducted before the experiments. Standard gas mixtures, delivered by Air Liquide, are used for the calibration of light species representing C_1-C_5 hydrocarbons except for diacetylene (C_4H_2) and triacetylene (C_6H_2) where their calibration factors are obtained from high-temperature acetylene (C_2H_2) pyrolysis experiments through carbon atom conservation. Likewise, liquid fuels, including benzene, toluene, styrene and phenylacetylene, are calibrated with mixtures prepared in stainless steel vessels by partial pressure method. On the other hand, for small PAHs up to three rings, calibrations are performed with gas-phase mixtures prepared in a heated glass vessel (200 °C) to minimize the surface absorption [48], and the detailed procedure is explained in [38]. Four-ring PAHs (pyrene and fluoranthene) cannot be steadily vaporized with the above approach. Therefore, their calibration factors are determined through an extrapolation from those of the two- and three- ring PAHs, namely, naphthalene, fluorene and phenanthrene. The liquid PAH standards are purchased from Sigma-Aldrich. The uncertainty in the concentrations measurements is expected to be within 5% for directly calibrated small species, 10–15% for PAH species calibrated in gas phase, and an error up to 50% for four-ring PAH species. Detailed information about the uncertainty of the PAH species measured in the current work is provided in **Table S1**.

For the chemicals used in the experiments, benzene (with a purity of 99.8%) and propyne (with a purity of 97%) are purchased from Sigma-Aldrich, while the gasses, including acetylene (>99.5%), ethylene (>99.5%), propylene (99.5%), argon (>99.9999%) and helium (>99.995%), are supplied by Air Liquide. Before use, benzene was purified by a series of freeze-thaw cycles to remove air, light gasses, and small impurities dissolved in the fuel. A 450B Matheson gas purifier with a 454 cartridge is connected to the acetylene bottle to remove the possible acetone traces, and acetone is found to be below the detection limit of the GC system in all the experiments (less than 0.1 ppm). The experimental gas mixtures are prepared in a 136 L electro-polished stainless-steel cylinder which is initially evacuated below 10^{-5} mbar with a turbo-molecular pump. Before running experiments, the prepared gas mixtures stay overnight to homogenize, and the actual pre-shock compositions are analyzed with the GC. Five argon diluted fuel experimental mixtures are used in the current work, including pure benzene, benzene-ethylene, benzene-acetylene, benzene-propylene, and benzene-propyne mixtures. The detailed compositions of the experimental mixtures are listed in **Table 2.** Some of the fuels' mixtures contain impurities, which have been measured to be methane (1.7 ppm) in the benzene-acetylene mixture, propane (1.6 ppm) in the benzene-propylene mixture, and 1-butyne (1.5 ppm), 1-butene (0.158 ppm), 2-butene (3.31 ppm), isobutene (0.134 ppm), isobutane (3.15 ppm) and ethylbenzene (0.53 ppm) in the benzene-propyne mixture (see Table 3). Before each experiment, the driven section of the shock tube is pumped to below 10^{-5} mbar before being filled with the experimental mixture. All experimental results, consisting of the post-shock conditions (T_5, p_5), the measured pressure profiles, the defined reaction time, and the mole fraction measurements for individual species, are provided in the ***Supplementary Material.***

3. Kinetic modeling

The detailed kinetic model for benzene-C_2/C_3 mixtures consisting of 552 species and 4958 reactions is developed by extending our previous serial works [15,38–40] that can well predict the PAH formation from benzene, toluene, C_8−C_{10} alkylbenzenes, binary phenylacetylene-C_2 mixtures, binary toluene-C_2 mixtures, propylene and propyne pyrolysis. Since the latest CRECK model by Pejpichestakul et al. [49] was selected as a starting point for our model development [15], the C_6H_5 sub-mechanism was already included in the core mechanism of the ongoing kinetic-model. It is noteworthy to point out that CRECK mechanism appears to match data despite the usage of the outdated kinetics for C_6H_5 dissociation through ring-opening [14]. No modifications are made for the single-ring aromatic chemistry as the PAH formation is focus of our serial works [15,38–40]. **Tables S2 and S3** in the ***Supplementary Material*** lists all the reactions added and updated in this work together with their rate coefficients and their sources. For the added reactions, the thermodynamic data of the corresponding species have been introduced. **Table S4** in the ***Supplementary Material*** provides the names, molecular formulas, and structures of the main involved species in the mechanism. Some key reactions that have been introduced and updated in the current model based on recent theoretical studies are described below.

The reactions sequence leading to the formation of 1,2-diethynyl benzene starting from phenylacetylene are updated from the theoretical work of Liu et al. [50]. Likewise, the reaction sequence: phenylacetylene ($C_6H_5C_2H$) +phenyl (C_6H_5) → phenanthrene ($PC_{14}H_{10}$) or diphenylacetylene ($C_6H_5CCC_6H_5$) and the relevant rate coefficients reported in a recent work by Tuli and Mebel [51] are included in the current model. The consumption of naphthalene ($C_{10}H_8$) occurs mainly via the H-atom abstraction reactions to form 1-naphthyl ($C_{10}H_7$_1) and 2-naphthyl ($C_{10}H_7$_2) radicals. The hydrogen abstraction rate coefficient of $C_{10}H_8$ by H is updated by the value recommended by Liu et al. [50]. The $C_{10}H_7$_1 can be converted to $C_{10}H_7$_2 through isomerization reaction. This pressure-dependent step is considered with rate constants taken from the work of Chu et al. [52]. Pressure-dependent reactions of acenaphthyl ($C_{12}H_7$), 1-ethynylnaphthyl, and 2-ethynylnaphyl radicals with C_2H_2 leading to the formation of ethynyl acenaphthylene and diethynyl naphthalene, respectively, were included in the model [52]. Rate coefficients for the unimolecular decomposition and hydrogen abstraction reactions by H of acenaphthylene, 1-ethynylnaphthylene and 2-ethynylnaphthylene are also introduced based on the same publication. Reaction rates of phenanthryl radicals with C_2H_2 to form ethynyl phenanthrene were taken from [50]. The reactions of acenaphthyl radicals, $C_{10}H_7$_1, $C_{10}H_7$_2, and C_6H_5 with diacetylene (C_4H_2) were added in an analogy to the reaction: $C_6H_5+C_2H_2=C_6H_5C_2H+H$ [21].

Based on the experimental work by Zhao et al. [53] via a high temperature chemical micro reactor coupled to Synchrotron-based tunable vacuum ultraviolet mass spectrometry, Oleinikov et al. [54] studied the growth mechanism of PAHs via reactions of 1- and 2-naphthyl with propyne and allene (C_3H_4-A) without providing reaction rate coefficients, as the authors only discuss the possible reaction pathways and products that can result from the reaction between naphthyl radicals and C_3H_4-P/C_3H_4-A. In this study, we adopted the rate constants analogously to the reactions of phenyl radical with propargyl (C_3H_3) and the reactions of phenyl radical with C_3H_4-P/C_3H_4-A from the theoreti-

Table 2
Compositions of the gas mixtures used for experiments.

Gas mixture	Composition Benzene(C_6H_6)	Ethylene (C_2H_4)	Acetylene (C_2H_2)	Propylene (C_3H_6)	Propyne (C_3H_4)
B	109 ppm	–	–	–	–
BE	108 ppm	532 ppm	–	–	–
BA	108 ppm	–	500 ppm	–	–
BPene	110 ppm	–	–	531 ppm	–
BPyne	108 ppm	–	–	–	508ppm

Table 3
Impurities measured in benzene-acetylene, benzene-propylene, and benzene-propyne mixtures.

Gas mixture	Impurities
BA	Methane (CH_4)=1.7 ppm
BPene	Propane (C_3H_8)=1.6 ppm
BPyne	1-butyne (C_4H_6–1) =1.5 ppm, 1-butene (C_4H_8–1) = 0.158 ppm, 2-butene (C_4H_8–2) = 3.31 ppm, isobutene (IC_4H_8) = 0.134 ppm, isobutane (IC_4H_{10}) = 3.15 ppm and ethylbenzene ($C_6H_5C_2H_5$) = 0.53 ppm

cal studies of [28,33], respectively. In a similar manner, the reactions of 1- and 2-ethynyl naphthyl radicals, acenaphthyl radicals, and phenanthryl radical with C_3H_4-P/C_3H_4-A/C_3H_3 are added to the model. The 1-, 2- and 3-methyl indene can be formed from the reactions between methyl (CH_3) radical and indene. The rate constants of these reactions are taken from the theoretical work of Mebel et al. [28]. Reactions of C_6H_5+1-butyne (C_4H_6–1)/2-butyne (C_4H_6–2) in analogy to C_6H_5+C_3H_4-P, while CH_3+1-phenylpropyne /3-phenylpropyne ($C_6H_5C_3H_3$P_1/ $C_6H_5C_3H_3$P_3) in analogy to $C_6H_5C_2H$+CH_3 are introduced to account for the formation of 4-phenyl-1-butyne ($C_6H_5CH_2CH_2CCH$).

The thermochemical data for most species is from the latest version of CRECK model [49] since it is the basis of the current model [15]. For the species introduced by reactions added or updated, their thermochemical data originate from the work of Chu et al. [52], while for the species introduced by the added reactions via analogies, their thermochemical data are computed with the program THERM [55]. The kinetic model, including the reaction mechanism and the species thermochemical data, is provided in the ***Supplementary Material***.

All simulations in the present work are performed with the homogeneous reactor model of the software COSILAB [56] considering the fuels as well as the impurities as input data. The comparison with the simulations performed without impurities in the initial fuel mixtures shows that in the case of C_6H_6+C_3H_4-P the profiles affected are those for ethylene, propylene and the C_4 intermediates (**Fig. S2** contains the most affected species profiles), while no visible difference could be obtained for the PAH products. Concerning the products of the benzene + acetylene reactions, the profiles for propyne and indene are the most affected by the presence of the methane impurity (**Fig. S3**). Constant $p5$ of 20 bar and a nominal reaction time of 4 ms are used in simulating the speciation measurements with the current kinetic model. The constant pressure assumption typically used in simulating the speciation results sampled from single-pulse shock tube experiments is well justified [44,47]. Nevertheless, it has been suggested that specific reactions involving resonantly stabilized radicals can potentially proceed during the post shock quenching [46,57]. Simulations with measured pressure profiles up to 10 ms were performed for the all five sets. The time dependent concentrations of major products and important radicals are shown in **Figs. S4 and S5** in the ***Supplementary Material***. The currently investigated reaction systems do not produce large amounts of highly-stabilized radicals such as benzyl, so the influences of the reactions during the post-shock quenching are minor. The plateaus in the concentrations of the major products during quenching processes indicate that their formation is already completed by the defined reaction time.

4. Results and discussion

This section summarizes and discusses the findings from the present study. Up to 50 species are identified and quantified in each set of the shock tube pyrolysis experiments. The list for each fuel mixture is presented in **Table S5**. Most of the detected species are present in all the five sets, but with different abundance and formation temperature windows. In general, this model can well reproduce the decomposition and formation mole fraction profiles of the observed species, as will be illustrated later in this section. Furthermore, the model can better predict the experimental data compared to the previous model [40], as can be observed in **Figs. S6–S12** in the ***Supplementary Material***. In this section, the first step is to shed light on the influences of the added C_2 and C_3 fuels on benzene decomposition reactivity and small hydrocarbons speciation. The subsequent step is to reveal the influences of added C_2 and C_3 on the speciation patterns of C_6H_6 pyrolysis, with particular attention paid to the MAH and PAH formation pathways. To this end, the species pools and reaction schemes of C_6H_6 + C_2H_2, C_6H_6+C_2H_4, C_6H_6 + C_3H_6, and C_6H_6 + C_3H_4-P pyrolysis are compared with those of neat C_6H_6 pyrolysis.

4.1. Fuels decomposition and speciation of small hydrocarbons

First, the synergetic effects between the fuel components in relation to their decomposition reactivity are inspected. Concentration profiles of C_6H_6 in neat benzene and benzene+C_2 binary mixtures, and those of C_2H_2 and C_2H_4 when they have been added as initial components are shown in Fig. 1. The current model can well capture the C_6H_6 decomposition reactivity throughout the investigated temperature range in all the three separate cases (Fig. 1(a)). Both the experimental and the modeling results indicate that the consumption of C_6H_6 is slightly promoted when C_2H_2 and C_2H_4 are added. Sensitivity analysis at T_5 = 1487 K and P_5 = 20 bar where C_6H_6 starts decomposing (15% of fuel decomposition for the pure benzene case) is performed in order to reveal the chemical details responsible for the faster benzene decomposition in the binary blends, and the results are shown in Fig. 2. H + C_6H_6=H_2+C_6H_5 plays a dominant role in benzene consumption in all the three cases, and it has more pronounced effect in C_6H_6+C_2H_x pyrolysis due to the increased level of H atoms. According to the ROP analysis, the enhanced level of H atoms is stemmed from the combination reactions between C_6H_5 + C_2H_2 and C_6H_5 + C_2H_4, which also account to the benzene consumption in BA and BE pyrolysis, respectively.

C_2H_2 and C_2H_4 mole fractions evolve differently with temperature (see Fig. 2(b) and (c)). Model-predicted C_2H_2 and C_2H_4

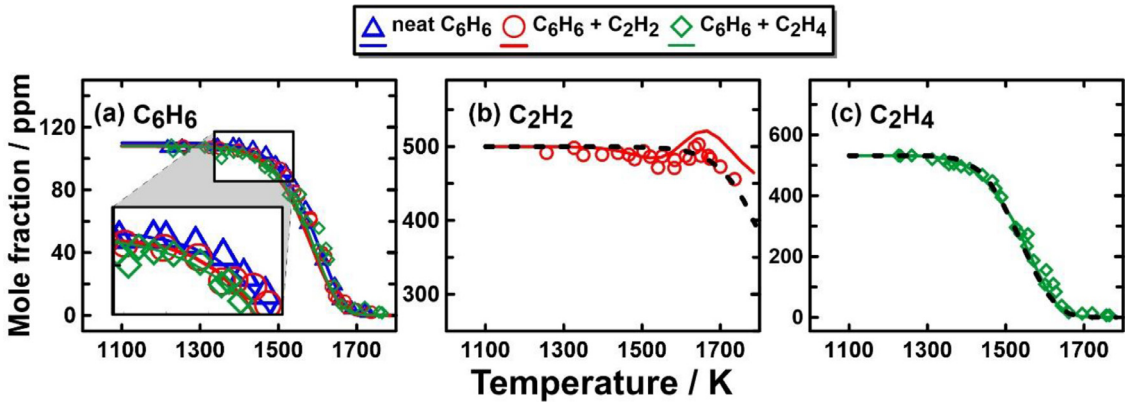

Fig. 1. Experimental (symbols) and simulated (solid lines) mole fractions of (a) C_6H_6 in the three investigated cases, (b) C_2H_2 in the pyrolysis of 108 ppm C_6H_6 + 500 ppm C_2H_2 mixture and (c) C_2H_4 in the pyrolysis of 108 ppm C_6H_6 + 532 ppm C_2H_4 mixture. The dashed lines in (b) and (c) represent the simulated mole fractions of C_2H_2 and C_2H_4 when C_6H_6 is absent from the corresponding mixtures.

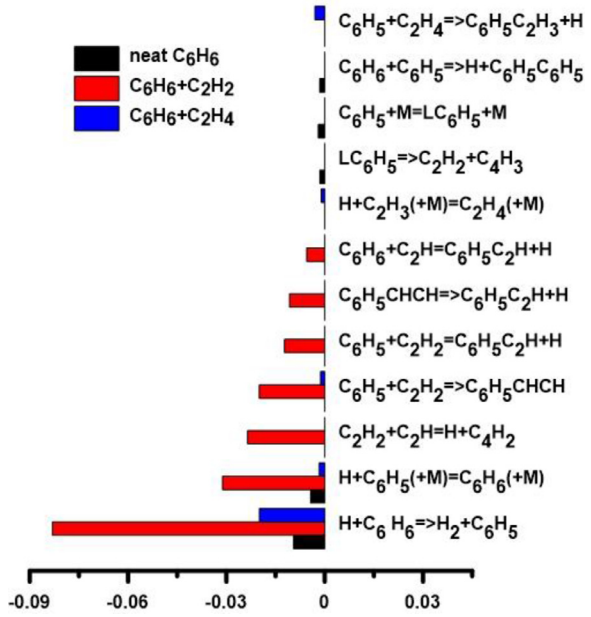

Fig. 2. Sensitivity analyses for C_6H_6 consumption at T_5 = 1487 K, P_5 = 20 bar and time=4 ms in the pyrolysis of neat C_6H_6, C_6H_6+C_2H_2 and C_6H_6+C_2H_4.

conversion curves when C_6H_6 is replaced with argon are also displayed in Fig. 2((b) and (c)) for comparison purpose and for easier visualization of the synergistic effects. The C_2H_2 decay in the temperature range of 1400–1500 K indicates a "synergistic effect" in the pyrolysis of C_6H_6+C_2H_2 mixture, which is caused via the reaction C_6H_5+C_2H_2 = $C_6H_5C_2H$ +H producing H atoms. The resulting H atom stimulates the consumption of C_6H_6 and C_2H_2 through the reactions H + C_6H_6=>H_2+C_6H_5 and C_2H_2+H = H_2+C_2H, respectively. The slight consumption of C_2H_2 above1500 K is compensated by its production from C_6H_5 decomposition at high temperatures. There is a slight over prediction by the model of the C_2H_2 formation above 1500 K, which can be mainly attributed to lack of consumption reactions to larger species than the ones considered in the current work since for the case of pure benzene the C_2H_2 is well predicted (see later in the section). In contrast, the presence of C_6H_6 barely changes the thermal decomposition rate of C_2H_4.

Concerning the synergistic effects of C_3 addition to benzene, mole fraction profiles of C_6H_6, C_3H_6 and C_3H_4-P in neat C_6H_6 and C_6H_6 + C_3H_x (x = 6, 4) pyrolysis experiments are shown in Fig. 3. As for Fig. 2, the dashed lines represent calculations performed without benzene in the initial mixture for comparison purposes. The current model can well capture the fuels' decomposition reactivity in all the three investigated cases. The added C_3H_6 and C_3H_4-P have different consequence on C_6H_6 consumption in the temperature range of 1260–1460 K, whereas benzene chemistry has insignificant impact on the decomposition rates of C_3 fuels (see Fig. 3(b) and (c)). C_3H_6 slightly promotes the C_6H_6 consumption in the temperature range of 1260–1360 K (no decay is observed in benzene pyrolysis case) followed by an increment in the C_6H_6 profile between 1360 and 1460 K (at lower extent compared to the C_3H_4-P + C_6H_6 case), and the subsequent steep fuel consumption at high temperatures. C_3H_4-P induces the C_6H_6 formation below 1460 K before the sharp decay of C_6H_6 at higher temperatures. To reveal the reasons behind this difference, rate-of-production (ROP) analyses for benzene are performed for both cases at T_5 = 1387 K where the increase in the profile has reached around 50% of its maximum value, and at T_5 = 1316 K where C_6H_6 is approaching its minimum in C_6H_6+C_3H_6 pyrolysis. The results of the analyses are presented in Fig. 4. At 1387 K, the C_3H_3 self-recombination is the main benzene formation path in C_6H_6+C_3H_4-P pyrolysis, in addition to the C_3H_4-A + C_3H_3 reaction, the isomerization/fragmentation of $C_5H_5CH_2$–1 and $C_5H_5CH_2$–2, and the isomerization of fulvene. Similar formation channels are also active in benzene+C_3H_6 case at 1316 K, but in this case the corresponding total production rates are not sufficient to compensate the benzene consumption through hydrogen abstraction reactions by H and CH_3, which are formed from the C_3H_6 decomposition. Indeed, the formation of C_3 precursors from C_3H_6 requires a stepwise dehydrogenation which is not so effective in the temperature range of 1260–1360 K. Hence, the belatedly C_3H_3 production and the abundance of CH_3 radicals and H atoms resulting from propylene decomposition contribute to the two-step phenomenon observed in C_6H_6+C_3H_6 pyrolysis in the low temperature region.

The results presented above highlight how the presence of C_2 fuels enhance the benzene decomposition due to the formation of H atoms (from C_6H_5 +C_2H_x reactions) and the subsequent reaction C_6H_6+H = C_6H_5+H_2. On the other hand, the addition of C_3 precursors leads to a rise in the benzene profiles below 1460 K through the C_3+C_3 reactions. Among the C_2 and C_3 hydrocarbons, only the acetylene profile is significantly affected by the presence of benzene, through H-atom abstractions by H to form C_2H + H_2 at temperatures below 1500 K, before the subsequent increase due to the fragmentation of the aromatic ring.

The second part of this section will focus on the formation of small hydrocarbons from the fuel decomposition. Concerning the formation of small hydrocarbons, Figs. 5 and 6 present the ex-

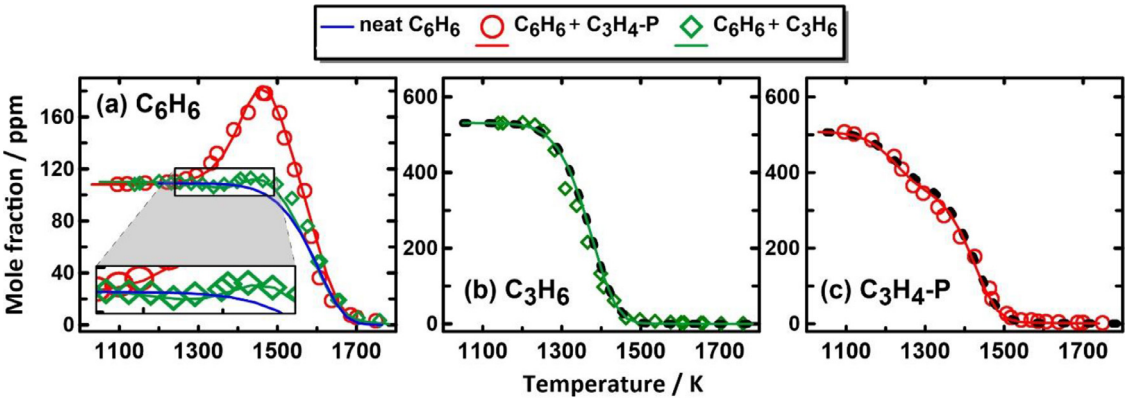

Fig. 3. Experimental (symbols) and simulated (solid lines) mole fractions of (a) C_6H_6 in the three investigated cases, (b) C_3H_6 in the pyrolysis of 108 ppm C_6H_6 + 532 ppm C_3H_6 mixture and (c) C_3H_4-P in the pyrolysis of 108 ppm C_6H_6 + 500 ppm C_3H_4-P mixture. The dashed lines in (b) and (c) represent the simulated mole fractions of C_3H_6 and C_3H_4-P when C_6H_6 is absent from the corresponding mixtures.

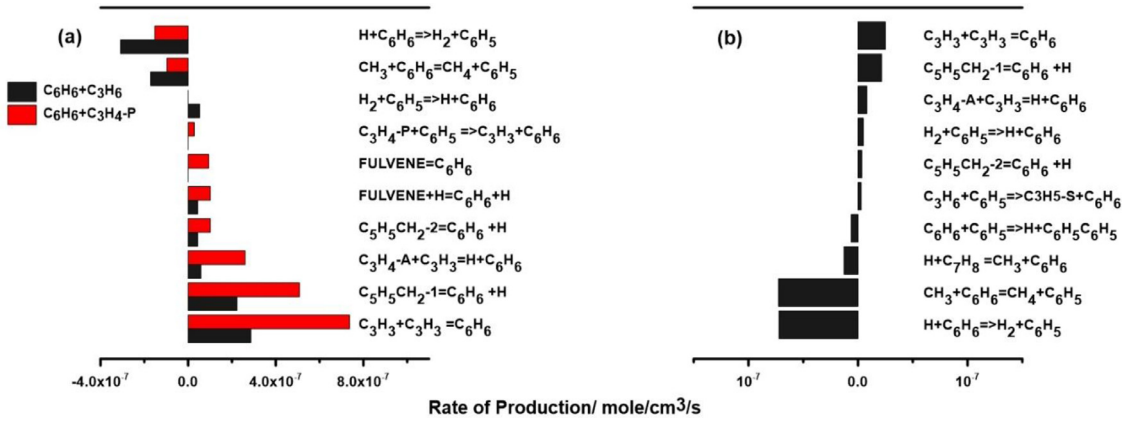

Fig. 4. Rate of production analyses at t = 4 ms for benzene in (a) C_6H_6+C_3H_6 and C_6H_6+C_3H_4-P pyrolysis at T_5 = 1387 K and (b) in C_6H_6+C_3H_6 pyrolysis at T_5 = 1316 K.

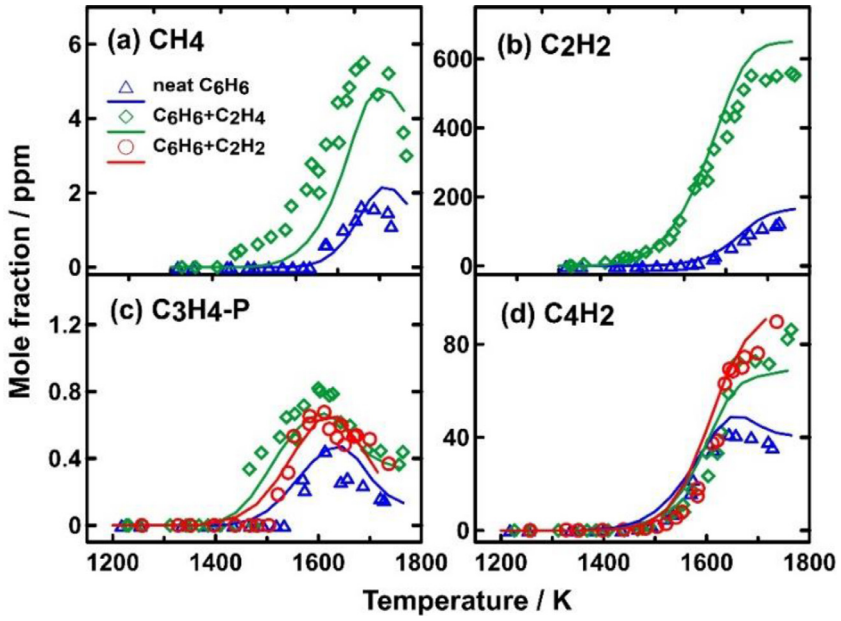

Fig. 5. Experimental (symbols) and simulated (lines) mole fraction profiles of methane (CH_4), acetylene (C_2H_2), propyne (C_3H_4-P) and diacetylene (C_4H_2) as a function of T_5 during the pyrolysis of 109 ppm C_6H_6, 108 ppm C_6H_6+ 500 ppm C_2H_2 and 108 ppm C_6H_6+532 ppm C_2H_4 mixtures.

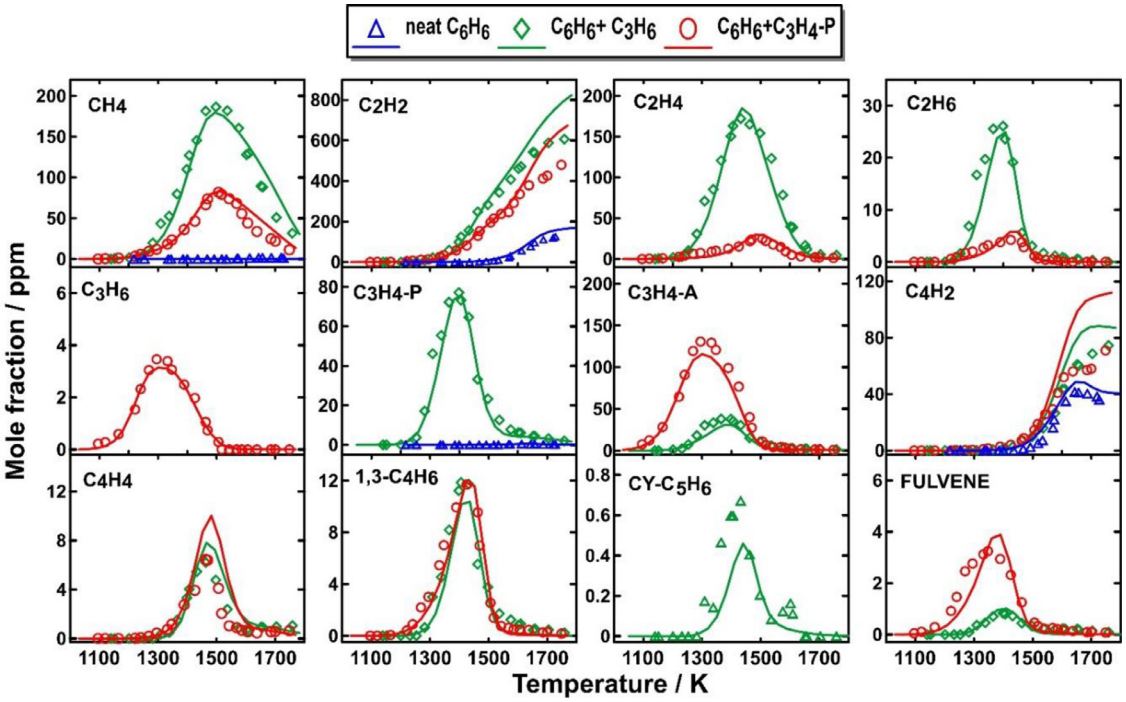

Fig. 6. Measured (symbols) and simulated (solid lines) mole fraction profiles of small hydrocarbon products as a function of T_5 during the pyrolysis of neat benzene, C_6H_6+C_3H_6 and C_6H_6+C_3H_4-P.

perimental and the simulated mole fraction profiles of C_1-C_6 non-aromatic hydrocarbons in the five sets. No modifications are made to the previous version of the model [40] to match the measurements for small hydrocarbons. In the case of benzene + ethylene reactions, the higher concentrations of CH_4, C_2H_2, and C_3H_4-P and their deviation to lower temperature windows compared to neat benzene arise from the breakdown of the unsaturated hydrocarbons. Similar considerations apply for the benzene + C_3. Moreover, the addition of C_2H_4, C_2H_2, C_3H_6 and C_3H_4-P contributes to the build-up of C_4H_2 mole fraction at elevated temperatures due to the increased number of carbon atoms in the initial mixture as well as the abundance of C_2H_2. Concerning specifically the systems with C_3 fuels, formation of large mole fractions of ethylene, ethane, allene, and C_4 HCs are observed, as well as propyne from the thermal fragmentation of propylene. In general, the profiles presented in Fig. 6 are qualitatively and quantitatively very similar to the ones presented in our previous work on the pyrolysis of propyne and propylene [40] as they derive almost exclusively from the decomposition of these fuels, thus the related kinetics will not be discussed in detail here.

4.2. Mono-aromatic hydrocarbon (MAH) formation

The presence of benzene and small unsaturated hydrocarbons in the initial fuel mixture favors the formation of various single-ring aromatics compared to the pure benzene case, where the small hydrocarbons can be formed only at high temperatures following the fragmentation of the ring. The mono-aromatic hydrocarbons are here presented to investigate the interactions between the different fuels and as the base for understanding the formation of larger PAH compounds. Quantitative measurements for MAH products and their corresponding simulations are presented in Figs. 7 and 8. The kinetic model can satisfactorily reproduce the measured MAHs mole fraction profiles in all the investigated reaction mixtures The addition of C_2 and C_3 fuels not only increases the amounts of the observed MAHs in neat benzene pyrolysis, but it also introduces new types of MAHs. The detected MAHs in these experiments mainly include phenylacetylene ($C_6H_5C_2H$), styrene ($C_6H_5C_2H_3$), toluene (C_7H_8), diethynyl benzene (C_6H_4 $(C_2H)_2$), 1-phenylpropyne ($C_6H_5C_3H_3$P_1), 4-phenyl-1-butyne ($C_6H_5CH_2CH_2CCH$), allyl benzene ($C_6H_5C_3H_5$–2), 1-phenylpropene ($C_6H_5C_3H_5$–1), methyl styrene ($CH_3C_6H_4C_2H_3$) and ethylbenzene ($C_6H_5C_2H_5$).

Phenylacetylene and diethynyl benzene are shared products in the five studied cases. The formation of $C_6H_5C_2H$ relies on the reactions between phenyl (C_6H_5) and C_2H_2/C_2H, and the formation of C_6H_4 $(C_2H)_2$ further relies on the reactions between phenylacetylene radical ($C_6H_4C_2H$) and C_2H_2. In neat benzene pyrolysis, the production of $C_6H_5C_2H$ is limited by the level of C_2H_2 that is mainly formed at elevated temperatures. This explains why the presence of C_2H_2 as fuel or its production from C_2H_4, C_3H_6, and C_3H_4-P decomposition shifts the formation of $C_6H_5C_2H$ and accordingly of C_6H_4 $(C_2H)_2$ to lower temperatures. The peak concentration of $C_6H_5C_2H$ is increased in all the binary mixtures, and, as expected, the addition of C_2H_2 exhibits the most pronounced effects. The maxima in the phenylacetylene profiles are around 16 ppm, 11–12 ppm, and 8 ppm for the acetylene, C_3, and ethylene addition, respectively. $C_6H_5C_2H_3$ is absent from the species pools of neat benzene and C_6H_6+C_2H_2 pyrolysis, and it mainly originates from the addition reactions between C_6H_6+C_2H_3 and C_6H_5+C_2H_4. The speciation temperature window for $C_6H_5C_2H_3$ is not significantly changed in the C_6H_6+C_2H_4 and C_6H_6+C_3H_6 pyrolysis, but it is shifted to higher temperatures in C_6H_6+C_3H_4-P pyrolysis. The late formation of $C_6H_5C_2H_3$ and the lower peak concentration in C_6H_6+C_3H_4-P pyrolysis are due to the limited production of C_2H_4 compared to C_6H_6+C_3H_6 pyrolysis.

All the following MAHs are absent from the species pools of neat benzene and benzene + C_2 pyrolysis. Toluene has higher peak concentration and lower temperature formation window in C_6H_6+C_3H_6 pyrolysis compared to C_6H_6+C_3H_4-P pyrolysis. To identify the reactions responsible for this difference, ROP analysis at 1400 K is performed for both cases where 50% of toluene is formed, and the results are shown in Fig. 9. C_7H_7+H + (M) =C_7H_8+ (M) is an efficient toluene

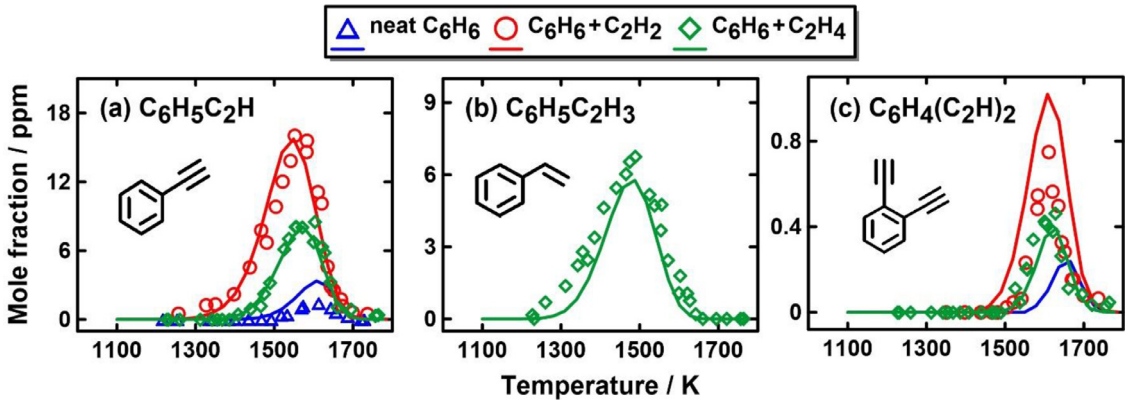

Fig. 7. Experimental (symbols) and modeling (solid lines) mole fractions of mono-aromatic hydrocarbons (MAHS) as a function of the post shock temperature T_5 in neat benzene and benzene+C_2H_x (x = 2, 4) pyrolysis.

formation channel when the H-atom level is considerable, and thus it accounts for 56.8% of toluene production in C_6H_6+C_3H_6 pyrolysis. As expected, if the H-atom concentrations diminish as for the case of benzene + propyne, the sensitivity coefficient for this reaction becomes negative as the overall reaction flux proceeds from toluene to benzyl. The reactions which primarily form C_7H_8 are the reactions of CH_3 with C_6H_6/C_6H_5, and the recombination reactions of C_3H_3 with but–2-yn-1-yl radical ($CH_2C\equiv CCH_3$) and 1, 3-butadiene. $C_6H_5C_3H_3$P_1 (Fig. 8(e)) and $C_6H_5C_3H_5$–1/$C_6H_5C_3H_5$–2 (Fig. 8(g) and (h)) are mainly the result of the recombination reactions of C_6H_5 with C_3H_4-P and C_3H_6, respectively. $C_6H_5C_2H$+CH_3 is the predominant $C_6H_5C_3H_3$P_1 source at elevated temperatures. $C_6H_5C_3H_3$P_1 starts to form at low temperatures in C_6H_6+C_3H_4-P because of the presence of C_3H_4-P in the initial mixture. The indirect formation of propyne and allene in C_6H_6+C_3H_6 pyrolysis leads to a lower peak concentration of $C_6H_5C_3H_3$P_1 and to a higher temperature production window. The trace quantities of $C_6H_5C_3H_5$–1 and $C_6H_5C_3H_5$–2 show that the interaction between C_6H_5 and C_3H_6 is not as efficient as C_6H_5 + C_3H_4-P. The reaction of methyl (CH_3) radical with $C_6H_5C_3H_3$P_1 exclusively contributes to the $C_6H_5CH_2CH_2CCH$ production in C_6H_6+C_3H_4-P pyrolysis. Other C_9 intermediates, like 3-phenyl-propyne ($C_6H_5C_3H_3$P_3) and phenyl-allene ($C_6H_5C_3H_3$A) are predicted to be major products of C_6H_5+C_3H_4-A and C_6H_5+C_3H_3/C_3H_4-P, respectively [22]. Both C_9H_8 isomers are under detection limits in the benzene+C_3 pyrolysis experiments, so the relevant reaction channels have limited importance. $CH_3C_6H_4C_2H_3$ (Fig. 8(i)) and $C_6H_5C_2H_5$ (Fig. 8(j)), detected only in C_6H_6+C_3H_6 pyrolysis, are mainly formed via the isomerization reaction of $C_6H_5C_3H_5$–1 through the intermediate indane (C_9H_{10}) and the recombination reaction C_7H_7 + CH_3, respectively.

The results presented in this section show how the presence of small hydrocarbons and their reaction with the aromatic ring structures leads to considerable concentrations of phenylacetylene and diethynyl benzene (for all cases), styrene (mainly for the C_6H_6 + C_2H_4 and + C_3H_6 cases, and toluene (for addition of C_3 fuels), which will influence the pathways of PAH formation as detailed in the next part of the manuscript. Other minor C_8, C_9, and C_{10} aromatics are formed in the case of C_3 addition.

4.3. PAH formation and growth

One crucial target of this work is to reveal the interactions between C_6H_6 and C_2/C_3 HCs, which alter the formation patterns of PAH species. It has already been shown how such interactions influence the single-ring aromatic pool. In this section, the different pathways to the multi-ring structures will be discussed and analyzed based on the experimental and modeling results.

Experimental and simulated mole fractions of the PAHs species (up to three-rings) are shown in Figs. 10 and 11 as a function of the temperature in the five investigated cases. All PAHs have higher mole fractions when C_2 and C_3 fuels are added to benzene except for biphenyl which derives from the reactions between two single-ring intermediates (phenyl + phenyl and phenyl + benzene). In general, the current kinetic model can satisfactorily reproduce the measurements for the PAH species regarding the peak concentrations and the formation temperature windows; however, it over predicts the peak concentrations for few major PAH species in C_6H_6+C_3H_4-P pyrolysis, such as naphthalene, acenaphthylene, and phenanthrene. There are two possibilities for this behavior, the kinetic rate constants for the formation reactions might be too high or the ones for the consumption pathways too low or missing. Based on the observations that can be made in this work, the latter hypothesis is the most probable as: 1) from a modeling point of view, the rate constants have been validated over a vast range of experimental profiles with different fuel components and mixtures[15,37–40]; 2) the early formation of the PAH species is well captured by the model, deviations appear only around the maxima (see Fig. 11); 3) the carbon recovery is much worst for the benzene + propyne case compared to addition of propylene or C_2s as shown in **Figs. S13 and S14** in the ***Supplementary Material***. Indeed, at high temperatures (T_5 = 1650 −1800 K) only around 50% of the carbon is recovered for the former case, against 75–85% in the other cases. It is important to underline the fact that the PAHs considered here only refer to the ones identified and quantified in the current experiments. Several three-to-four ring PAH peaks are detected but their structures could not be determined or the calibration could not be obtained in an accurate way (for the largest 4-ring structures). The carbon balance would be further improved if all the gas-phase products could be taken into consideration. Similar observations were done comparing propylene pyrolysis with propyne pyrolysis [40]. This suggests the propensity of propyne to form large PAHs and eventually soot particles compared to propylene.

As mentioned above, biphenyl is the only PAH species whose concentrations reduce in the binary mixture cases compared to the pure benzene one. The C_6H_6+C_6H_5 reaction bears a considerable carbon flux in the case of benzene pyrolysis. The resulting biphenyl ($C_6H_5C_6H_5$) is the most abundant PAH species in the corresponding case. However, the addition of C_2 and C_3 fuels shifts the $C_6H_5C_6H_5$ formation temperature window to higher temperatures and it lowers the peak concentration as shown in Fig. 10(e) and Fig. 11(f). C_6H_5 either decomposes or reacts with other radicals, including

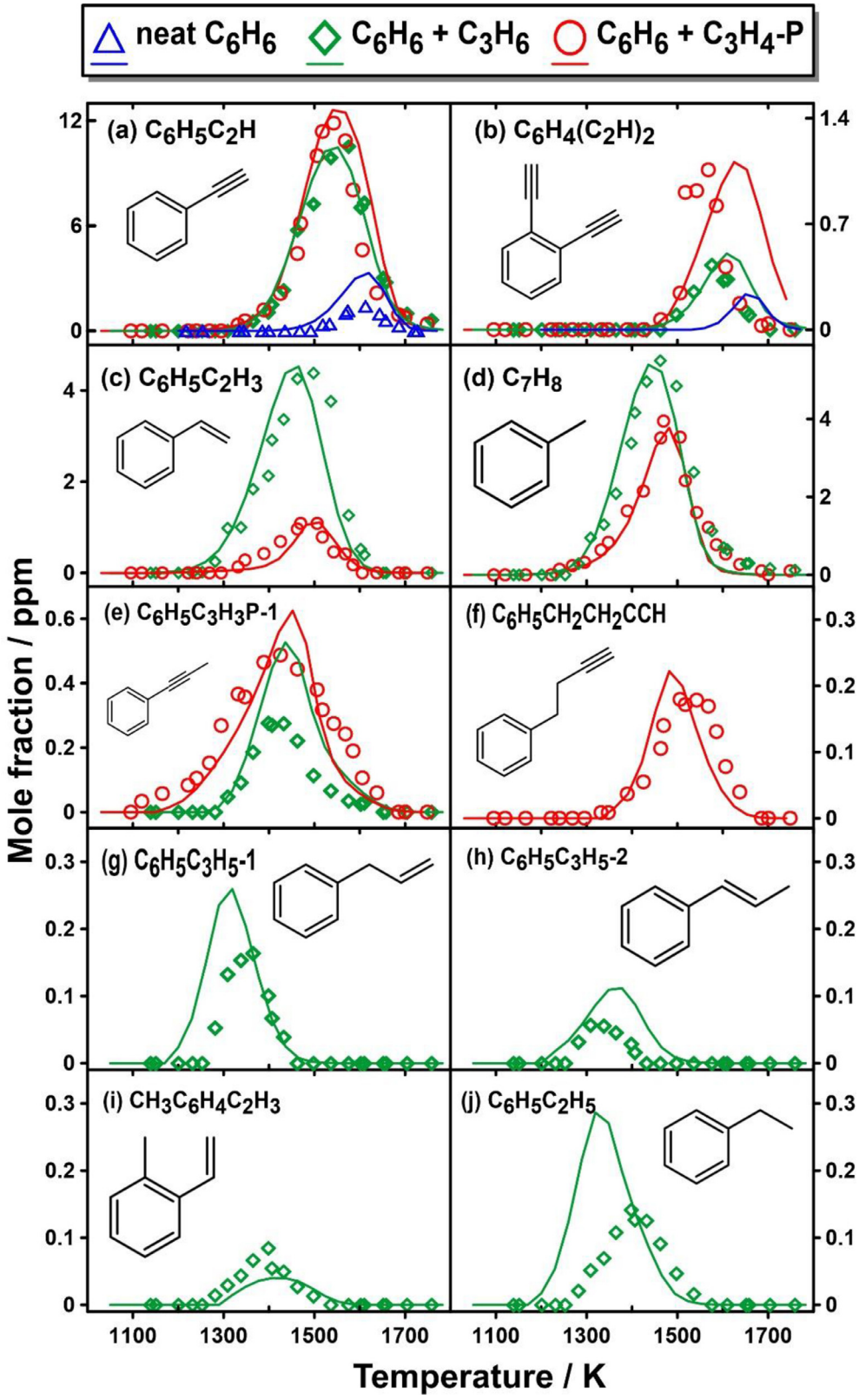

Fig. 8. Experimental (symbols) and modeling (solid lines) mole fractions of mono-aromatic hydrocarbons (MAHS) as a function of the post shock temperature T_5 in neat benzene and benzene+C_3H_x ($x = 4, 6$) pyrolysis.

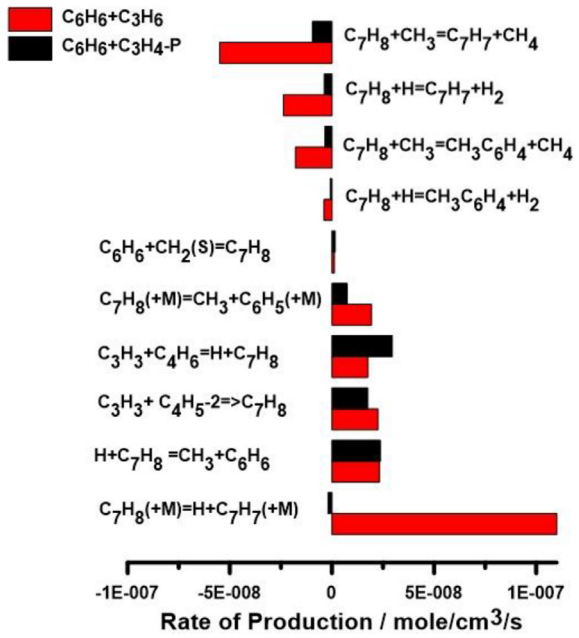

Fig. 9. Rate of production analysis at time=4 ms for toluene in C_6H_6+C_3H_6 and C_6H_6+C_3H_4-P pyrolysis at T_5=1400 K.

the C_2/C_3 fuels and C_6H_5 itself. The contributions of reactions involving C_2 and C_3 fuels increase notably in the binary mixtures. This is evident by the abundant observation of C_8 species in all five sets and the C_9 species in benzene/C_3 co-pyrolysis experiments, as discussed in the previous section. Thus, the C_6H_6+C_6H_5 pathway, which leads to $C_6H_5C_6H_5$ formation, is inhibited in the case of C_2/C_3 additions. Besides, the reaction between phenyl propargyl radical ($C_6H_4C_3H_3$) and C_3H_3 minorly contributes to $C_6H_5C_6H_5$ production in benzene/C_3 pyrolysis. The model slightly underpredicts the formation of biphenyl in benzene pyrolysis, suggesting that the phenyl concentration might be underestimated (probably due to its consumption by thermal decomposition). Considering the vast validation of the model against results obtained with other aromatic fuels, no further adjustments were considered. On the other hand, the biphenyl profiles for the binary mixtures are well reproduced.

One of the main point of interest in studying the reactions between the single-ring structures and the C_3 fuels is the validation of the pathways to indene. Indeed, indene (C_9H_8) is identified as a major C_9 product in both C_6H_6+C_3H_4-P and C_6H_6+C_3H_6 pyrolysis experiments (maximum mole fractions of around 3 ppm). The measured and simulated mole fractions of C_9H_8 are shown in Fig. 12 for the two investigated cases in comparison with those in neat benzene pyrolysis. The model can accurately reproduce C_9H_8 profiles in the three investigated cases. C_9H_8 formation mechanisms mainly include the isomerization of $C_6H_5C_3H_3$P_1 and $C_6H_5C_3H_3$A, the reaction of benzyl radical (C_7H_7) with C_2H_2, and the reaction of C_6H_6 with C_3H_3. The unimolecular decomposition of C_9H_{10} originating from $C_6H_5C_3H_5$–1 isomerization and the reaction of C_7H_7 with C_3H_4-P have a minor contribution to C_9H_8 formation. The addition of propene and propyne to benzene enhances the indene production but to a lower extent compared to the addition of acetylene to toluene [38] where more than 10 ppm of indene are produced at around 1450 K from the reaction between 105 ppm C_7H_8 and 459 ppm C_2H_2. This indicates that the indene formation in the benzene + C_3 co-pyrolysis is not as efficient as indene formation in the toluene + acetylene co-pyrolysis, where the resonantly stabilized benzyl radical reacts with the abundant acetylene present in the initial mixture to form directly indene + H. The addition of the C_2 fuels has limited influences on indene production, as in benzene-C_2 pyrolysis (Fig. 10a), indene is also mainly formed through the C_6H_6+C_3H_3 reaction, where C_3H_3 is the limiting factor.

Naphthalene ($C_{10}H_8$) is among the fused bicyclic PAH species with the highest concentrations in the five investigated cases. The addition of C_2H_4, C_3H_4-P, and C_3H_6 promotes the $C_{10}H_8$ formation and it lowers the formation temperatures, with maximum mole

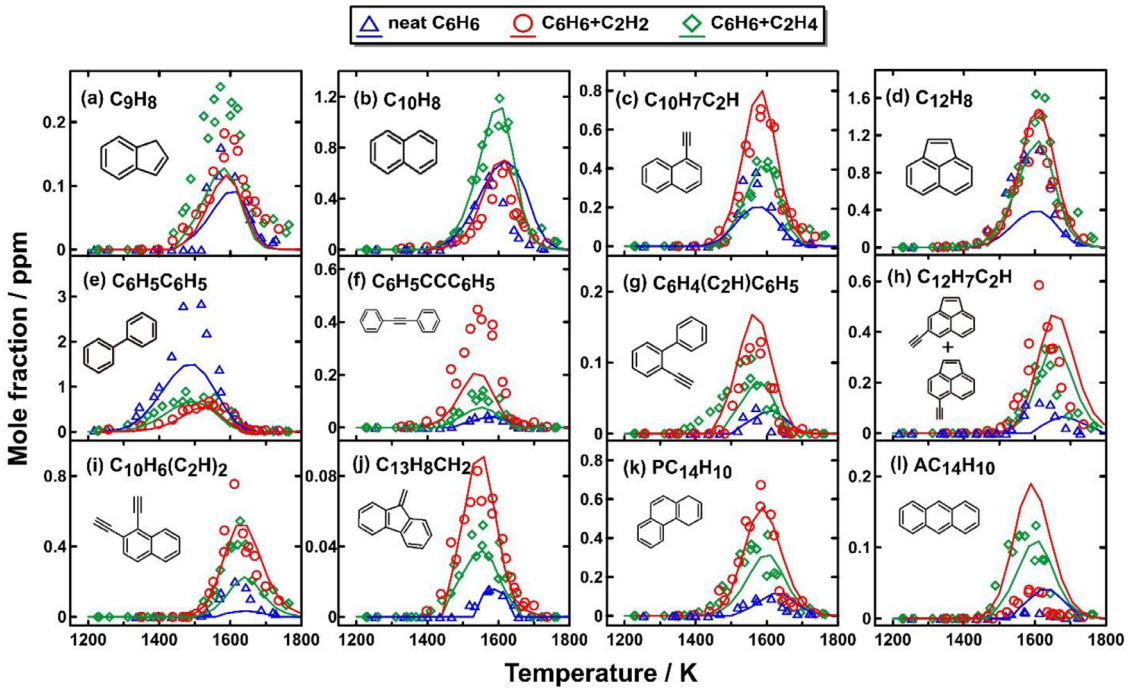

Fig. 10. Experimental (symbols) and modeling (solid lines) mole fractions of polyaromatic hydrocarbons (PAHS) as a function of the post shock temperature T_5 in neat benzene, benzene+C_2H_2 and benzene+C_2H_4 pyrolysis.

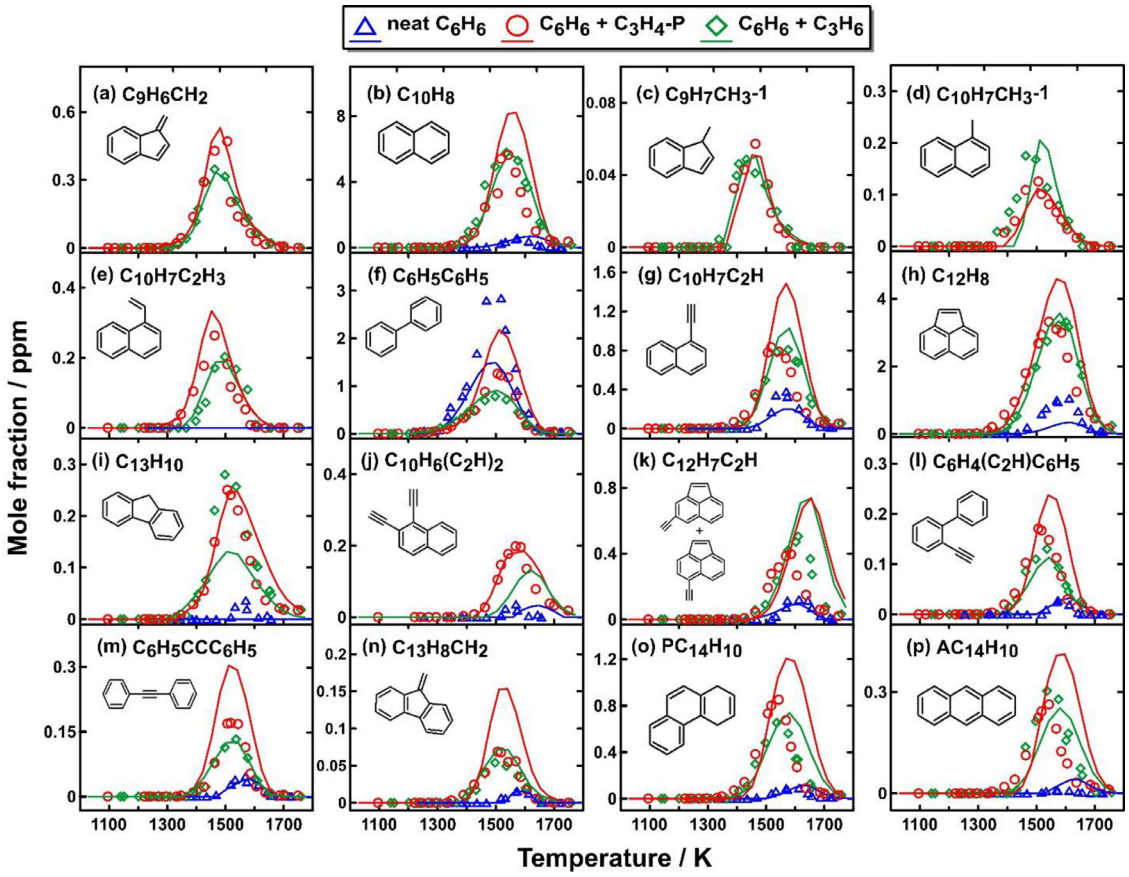

Fig. 11. Measured (symbols) and simulated (solid lines) mole fractions of poly-aromatic hydrocarbons (PAHs) as a function of the post shock temperature T_5 in neat benzene, benzene+C_3H_4-P and benzene+C_3H_6 pyrolysis.

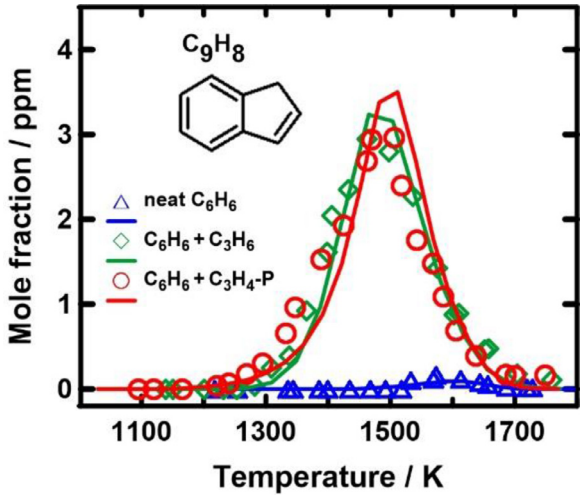

Fig. 12. Experimental (symbols) and modeling (solid lines) mole fractions of indene (C_9H_8) as a function of the post shock temperature T_5 in neat benzene, benzene+C_3H_4-P and benzene+C_3H_6 pyrolysis.

fractions of around 1.2 ppm, 5.5 ppm, and 5.5 ppm, respectively, compared to 0.6 ppm in the pure benzene pyrolysis. Thus, it is clear how the presence of the C_3 fuels enhances the pathways to the second-ring fused structure. The addition of C_2H_2 has almost negligible effects. This is mainly due to the lack of H-atom sources which makes the HACA route to naphthalene not efficient at these conditions [13]. To obtain detailed kinetic insights into the remarkable influence of the extra C_2H_4, C_3H_4-P and C_3H_6 on $C_{10}H_8$ formation, the reaction networks leading to naphthalene are shown in Fig. 13 based on the integrated ROP analysis at 1530 K, where considerable amounts of $C_{10}H_8$ are produced. The pathway of o-benzyne (o-C_6H_4)+C_6H_6 through the intermediate BICYCLO [58] is a dominant source of $C_{10}H_8$ in benzene (40% of the total integrated rate of production) and benzene/C_2 pyrolysis (10–18% of the rate of production), while it has minor contribution to $C_{10}H_8$ formation throughout the whole temperature range in benzene/C_3 pyrolysis. The HACA pathway through $C_6H_4C_2H$ leading to naphthyl radical ($C_{10}H_7$_1) is important for all the cases studied in terms of percentage contribution to $C_{10}H_8$, with the absolute flux depending on the concentrations of H-atom sources (H or H_2, C_6H_6, and C_2H_4 in the benzene + ethylene case). The $C_{10}H_7$_1 + C_2H_4 pathway also leads to the production of vinyl naphthalene ($C_{10}H_7C_2H_3$), for which the measured and simulated mole fraction profiles are shown in Fig. 14. $C_{10}H_7C_2H_3$ is also present in benzene/C_3 pyrolysis (Fig. 11(e)), but in this case it originates mainly from the reaction of C_9H_7 with C_3H_3. $C_{10}H_7C_2H_3$ can thermally decompose to naphthalene + vinylidene. The ipso-substitution reaction between $C_{10}H_7C_2H_3$ and H atom also leads to $C_{10}H_8$ + C_2H_3, mainly in the benzene +ethylene co-pyrolysis (pathway not shown in Fig. 13).

Among the other C_{10} products, in the benzene + acetylene, propyne, and propylene cases, the pathways involving benzo fulvene ($C_9H_6CH_2$) play a dominant role in the naphthalene formation. Benzo fulvene was measured in the benzene + C_3 cases (Fig. 11a) while in the case of acetylene addition the peak size was close to our detection limit (estimated maximum mole fraction of around 10^{-2}). The formation of $C_9H_6CH_2$ is due to different formation pathways in the binary mixtures. In benzene/C_3 pyrolysis, it relies on four major channels: i) the decomposition of $C_9H_6CH_3$–1; ii) the recombination reaction of C_7H_5 with C_3H_3; iii) the bi-

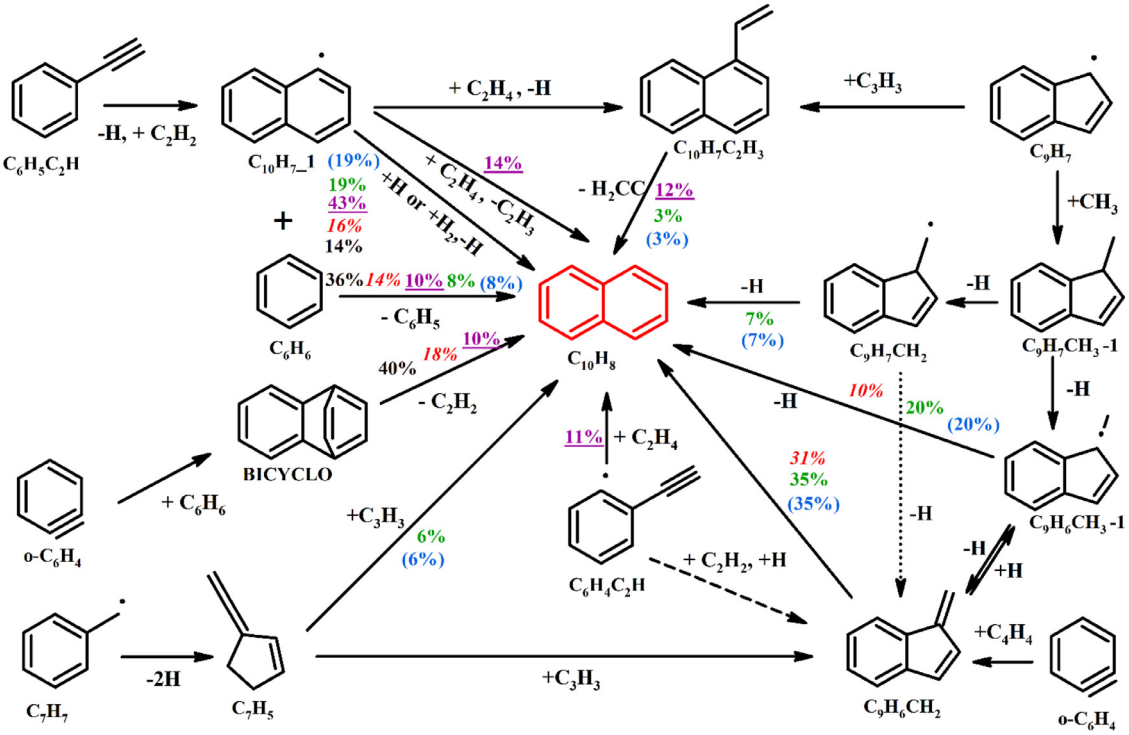

Fig. 13. The reaction pathways leading to naphthalene formation based on integrated ROP analyses at T_5 of 1530 K in the pyrolysis of benzene, benzene/C_2, and benzene/C_3 binary mixtures. The percentage numbers (B: black normal; BA: red italic; BE: purple underlined; BPene: green normal; BPyne: blue in brackets) represent the contributions of the corresponding reactions in naphthalene formation. The dashed arrow resembles multi-step reactions.

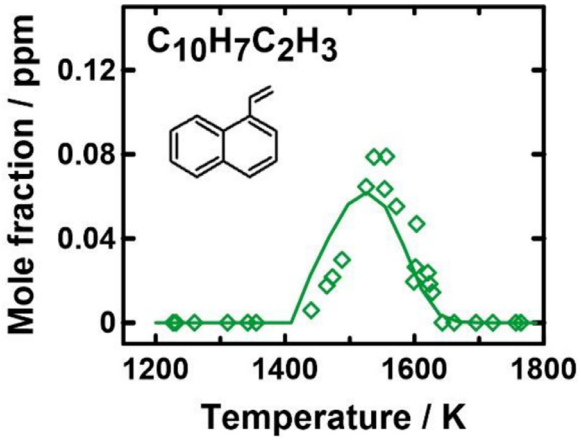

Fig. 14. Experimental (symbols) and modeling (solid lines) mole fractions of vinyl naphthalene as a function of the post shock temperature T_5 in benzene+C_2H_4 pyrolysis.

molecular reaction between o-C_6H_4 and vinylacetylene (C_4H_4); iv) the HACA reaction between $C_6H_4C_2H$ + C_2H_2 leading to benzofulvenyl radical (C_9H_6CH) which further reacts with H atom. Differently, in benzene/C_2 pyrolysis, it is solely produced via the HACA pathway starting from $C_6H_4C_2H$. Direct isomerization of $C_9H_6CH_2$ to $C_{10}H_8$ accounts for around 31–35% of the total naphthalene formation in the C_6H_6 + C_2H_2, C_3H_4-P and C_3H_6 systems. The addition of H atom to $C_9H_6CH_2$ leads to $C_9H_6CH_3$–1 radical which consequently decomposes to $C_{10}H_8$ in benzene+C_2H_2 pyrolysis. Likewise, the unimolecular decomposition of $C_9H_6CH_3$–1 following the production of 1-methyl indene ($C_9H_7CH_3$–1) through C_9H_7 + CH_3 also accounts for $C_{10}H_8$ formation in benzene/ C_3 co-pyrolysis. Other relevant pathways to naphthalene for the benzene + C_3 reactions are i) the recombination reaction between fulvenallyl (C_7H_5) and C_3H_3, where C_7H_5 mainly comes from C_7H_7 decomposition; ii) the decomposition of $C_9H_7CH_2$ forming $C_{10}H_8$ + H, $C_9H_7CH_2$ being produced from the dehydrogenization of methyl indene; iii) the ipso-substitution reaction between 1-methyl naphthale ne ($C_{10}H_7CH_3$_1) and H atom forming $C_{10}H_8$ + CH_3 (not shown); $C_{10}H_7CH_3$_1 is the product of the bimolecular reactions between $C_{10}H_7$_1 and CH_3. Finally, in C_6H_6+C_2H_4 reaction system, the reaction between $C_6H_4C_2H$ and C_2H_4 produces an adduct $C_6H_4(CHCH_2)(CHC\dot{H})$, which subsequently undergoes ring closure step forming $C_{10}H_8$ and releasing a hydrogen atom. This channel results in the higher observed $C_{10}H_8$ mole fractions by skipping $C_{10}H_7$_1 formation at low temperatures.

Another major PAH intermediate whose production is enhanced by the cross reactions between benzene and the small hydrocarbons fuels is acenaphthylene. An increase in acenaphthylene ($C_{12}H_8$) peak concentration from 1 ppm for pure benzene to 1.5 ppm for benzene + C_2 (Fig. 10(d)) and to 3 ppm for benzene + C_3 (Fig. 11(h)) is observed. The extra C_3 not only has more obvious promoting effects on $C_{12}H_8$ peak, but it also tends to shift its formation temperature window to lower temperatures. The model is capable to predict the formation of acenaphthylene for the mixtures but it under-predicts the peak mole fraction for pure benzene, which once again may suggest the need of further refinements for the phenyl radical decomposition steps. The formation scheme of $C_{12}H_8$ based on the integrated ROP analyses results at 1500 K is shown in **Fig. 15**. Two major pathways contribute to $C_{12}H_8$ formation in all cases: i) the isomerization of biphenyl radical ($C_{12}H_9$) through cyclopenta [a] indene (BENZO) intermediate; ii) the HACA route through C_6H_5→ $C_6H_5C_2H$ → naphthyl ($C_{10}H_7$_1) → $C_{12}H_8$. The latter one relies on two important precursors, $C_{10}H_7$_1 and C_2H_2. C_2H_2 concentration is limited in neat benzene pyrolysis. The existence of C_2H_2 as a fuel or being produced from C_2H_4, C_3H_4-P, and C_3H_6 decomposition intensifies the HACA pathway in the binary mixtures. Furthermore, the level of $C_{10}H_7$_1 resulting from $C_{10}H_8$ decomposition is higher in C_3 binary

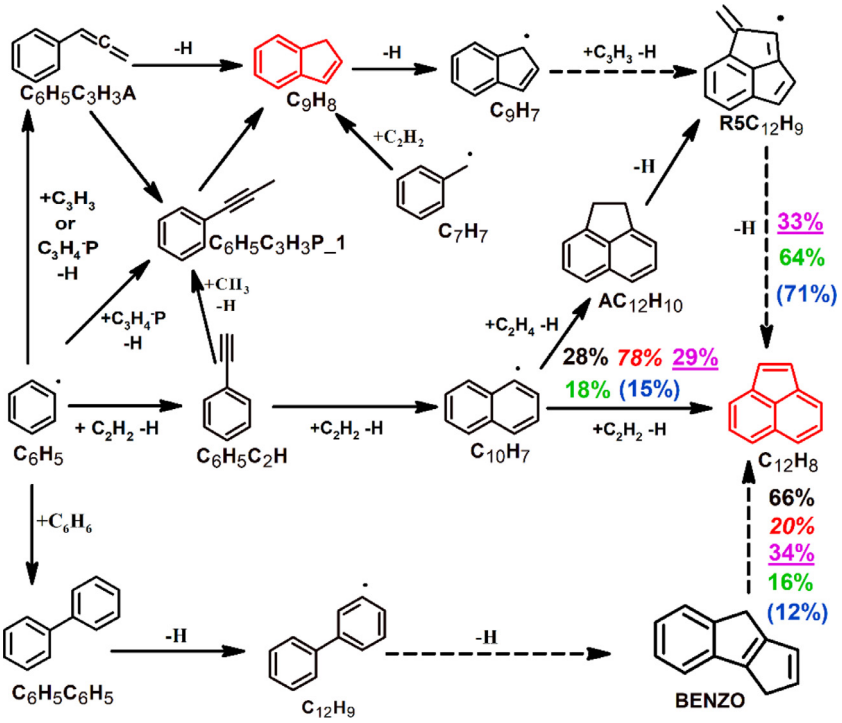

Fig. 15. The reaction pathways leading to acenaphthalene formation based on integrated ROP analyses at T_5 of 1500 K in the pyrolysis of benzene, benzene/C_2, and benzene/C_3 binary mixtures. The percentage numbers (B: black normal; BA: red italic; BE: purple underlined; BPene: green normal; BPyne: blue in brackets) represent the contributions of the corresponding reactions in acenaphthylene formation. The dashed arrows indicate multiple step processes.

mixtures, which improves the efficiency of the $C_{10}H_7$_1 + C_2H_2 reaction leading to $C_{12}H_8$. In C_6H_6+C_2H_4 pyrolysis, $C_{10}H_7$_1 can also react with C_2H_4 producing acenaphthene ($AC_{12}H_{10}$) which decomposes into $C_{12}H_8$ through the $R5C_{12}H_9$ intermediate. The other channel through C_9H_7 + C_3H_3, proposed recently by Jin et al. [59], is the governing formation pathway of $C_{12}H_8$ at low temperatures in both C_6H_6 + C_3H_6 and C_6H_6 + C_3H_4-P pyrolysis (64% and 71%, respectively).

We have seen how the HACA route is one of the major driving forces for the formation of phenylacetylene and acenaphthylene in the case of the binary mixtures. The reactions between aromatic radicals and acetylene also leads to other PAHs with ethynyl moieties. For example, the formation of 1-ethynylnaphthalene ($C_{10}H_7C_2H$_1, Fig. 10(c) and Fig. 11(g)) follows the same HACA route pathway as that of $C_{12}H_8$. Minor $C_{10}H_7C_2H$_1 formation pathways include the $C_{10}H_7$_1 + C_3H_4-P reaction in C_3 binary mixtures (3% in BPyne pyrolysis and 2% in BPene pyrolysis at 1470 K). Besides, the HACA route through acenaphthylene radicals ($C_{12}H_7$) + C_2H_2 and ethynyl naphthalene ($C_{10}H_6C_2H$) radicals + C_2H_2 leads to ethynyl acenaphthalene ($C_{12}H_7C_2H$, Fig. 10(h) and Fig. 11(k)) and diethynyl naphthalene ($C_{10}H_6(C_2H)_2$, Fig. 10(i) and Fig. 11(j)), respectively. According to the results of ROP analyses, the formation of the above-mentioned $C_{14}H_8$ isomers largely depends on $C_{12}H_7$/$C_{10}H_6C_2H$ + C_2H_2 reactions. The higher abundance of C_2H_2 at low temperatures explains the higher concentration and the lower formation temperature window of the $C_{14}H_8$ isomers in the pyrolysis of the binary mixtures (Fig. 10 (h and i) and Fig. 11 (j and k)).

In addition to the major PAH species discussed in the previous paragraphs which are common to both the benzene + C_2 and benzene + C_3 mixtures, different types of C_{10}-C_{13} PAHs including $C_9H_7CH_3$, $C_{10}H_7CH_3$_1, $C_{10}H_7C_2H_3$, and fluorene ($C_{13}H_{10}$) are detected in benzene/C_3 pyrolysis. Their mole fraction profiles are shown in Fig. 11. $C_9H_7CH_3$ and $C_{10}H_7C_2H_3$ are formed mainly from the reaction of C_9H_7 with CH_3 and C_3H_3, respectively. Both $C_9H_7CH_3$ and $C_{10}H_7C_2H_3$ are naphthalene precursors as discussed in the previous paragraph; however, $C_9H_7CH_3$ is an important formation precursor for both $C_{10}H_8$ and $C_9H_6CH_2$. The reactions of naphthyl ($C_{10}H_7$_1) radical with CH_3 controls the formation of $C_{10}H_7CH_3$_1. The dominant formation pathways for $C_{13}H_{10}$ in these two investigated sets are the addition reactions of C_3H_4-P to $C_{10}H_7$_2 and C_4H_4 to C_9H_7. The reaction sequence biphenylmethane ($C_{13}H_{12}$) →$C_{13}H_{11}$→$C_{13}H_{10}$ also has a slight contribution to the production of $C_{13}H_{10}$.

The final part of this discussion will be focused on the larger molecules quantified in the present work, in particular on the $C_{14}H_{10}$ isomers. Both Fig. 10 (f, g, j, k and l) and Fig. 11 (i, m, n, o and p) display the mole fraction profiles of the five isomers, namely, ethynyl biphenyl (C_6H_4 (C_2H) C_6H_5), diphenylacetylene ($C_6H_5CCC_6H_5$), 9-methylene-fluorene ($C_{13}H_8CH_2$), phenanthrene ($PC_{14}H_{10}$), and anthracene ($AC_{14}H_{10}$). The addition of the C_2 and C_3 compounds increases the peak concentration of all the five isomers and leads to their early formation. Reaction pathways leading to the $C_{14}H_{10}$ isomers formation at 1530 K are presented in Fig. 16. The enhanced formation of all the $C_{14}H_{10}$ isomers is supported by the increased $C_6H_5C_2H$ formation, since it largely depends on the $C_6H_5C_2H$+C_6H_5 reactions. $PC_{14}H_{10}$, the most dominant $C_{14}H_{10}$ isomer, mainly comes from the H-assisted isomerization of $C_6H_5CCC_6H_5$ and $C_{13}H_8CH_2$ and the decomposition of $C_6H_5C\dot{C}HC_6H_5$ radical produced by addition of an H atom to $C_6H_5CCC_6H_5$. $AC_{14}H_{10}$ is mostly formed through the isomerization of $PC_{14}H_{10}$. The naphthyne ($C_{10}H_6$–23) + C_6H_6 reaction (CAF route [60]) and the C_7H_5 self-recombination have minor contribution to $AC_{14}H_{10}$ formation in neat benzene and benzene/C_2 and benzene/C_3 pyrolysis, respectively. C_6H_4 (C_2H) C_6H_5, $C_6H_5CCC_6H_5$ and $C_{13}H_8CH_2$ mainly originate from the $C_6H_5C_2H$+C_6H_5 reactions, which are the main source of the measured $C_{14}H_{10}$ PAH species as highlighted in our previous works [38,39]. The 1, 1-diphenylethylene ($C_6H_5C(CH_2)C_6H_5$) decomposition that is formed through $C_6H_5C_2H_3$+C_6H_5 has a supporting role in $C_{13}H_8CH_2$ for-

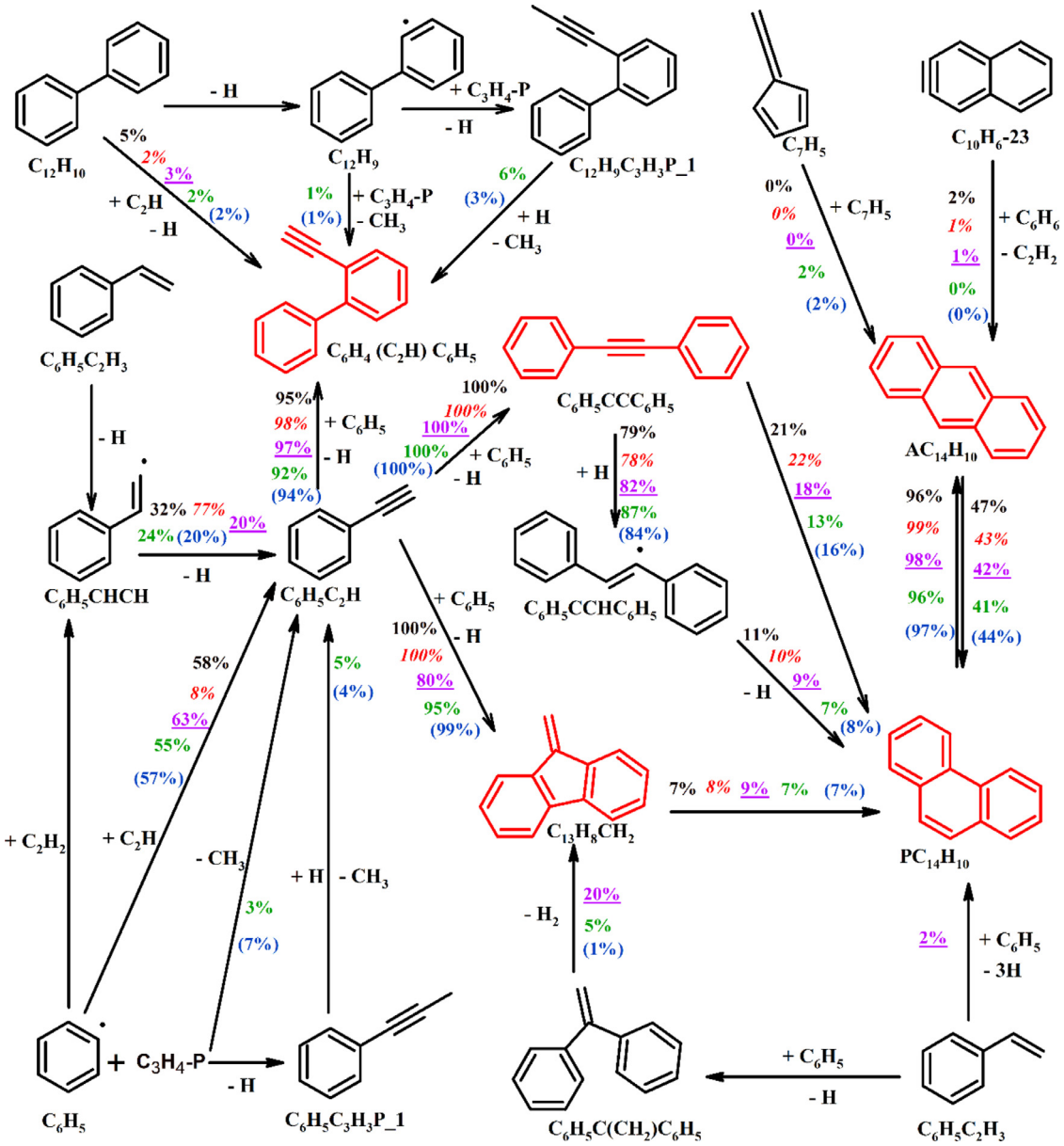

Fig. 16. The reaction pathways leading to the formation of $C_{14}H_{10}$ isomers based on integrated ROP analyses at T_5 of 1530 K in the pyrolysis of benzene, benzene/C_2, and benzene/C_3 binary mixtures. The percentage numbers (B: black normal; BA: red italic; BE: purple underlined; BPene: green normal; BPyne: blue in brackets) represent the contributions of the corresponding reactions in $C_{14}H_{10}$ formation.

mation in C_6H_6+C_2H_4 pyrolysis while a limited role in benzene/C_3 pyrolysis. There are additional pathways that contribute to C_6H_4 (C_2H) C_6H_5 formation. C_6H_4 (C_2H) C_6H_5 is trivially produced through the reaction channel: $C_6H_5C_6H_5$+C_2H= C_6H_4 (C_2H) C_6H_5 +H in all the reaction systems. Besides, in benzene/C_3 pyrolysis, the reaction of $C_{12}H_9$ with C_3H_4-P leads either directly to C_6H_4 (C_2H) C_6H_5 formation or to 1-biphenyl propyne ($C_{12}H_9C_3H_3P$_1) which subsequently reacts with H to form C_6H_4 (C_2H) C_6H_5 + CH_3.

5. Conclusion

This article presents a detailed experimental and modeling investigation on the single-pulse shock tube pyrolysis of C_6H_6, C_6H_6 + C_2H_2, C_6H_6+C_2H_4, C_6H_6 + C_3H_6, and C_6H_6 + C_3H_4-P at a nominal pressure of 20 bar over a temperature range of 1030–1800 K. The pyrolysis products including small hydrocarbons and PAHs are identified and quantified using the GC/GC–MS technique. An on-going kinetic model is further developed based on the recent theoretical progresses and validated against the current experimental data, as well as the previous experimental datasets. The model is capable to quite accurately simulate the experimental profiles for the fuels and the main pyrolytic products, including the PAH intermediates, although a general over-prediction is observed for several PAH species in the benzene + propyne case. These discrepancies are attributed to missing consumption pathways, as a worst carbon balance is observed for this specific case compared to the other fuel mixtures.

The comparison between the different sets allows for the first time to study in detail the interaction between phenyl radical and the unsaturated hydrocarbons through joined experimental observations and modeling interpretations. In particular, the key reaction networks are revealed through ROP analyses for the investigated reaction systems. The synergistic effects observed in the benzene/C_2 binary mixtures concerning benzene decomposition derive from the H-abstraction reactions by H, while the addition of propyne leads to the formation of benzene through C_3+C_3 re-

actions, resulting in a rise of the benzene profile below 1460 K. For the benzene + propylene case, for temperatures between 1260 and 1360 K, the H-abstraction reactions dominate resulting in a slight decrement of the benzene mole fraction, while a subsequent increment is observed up to 1460 K due to the C_3+C_3 reactions. Among the small hydrocarbons added to the initial mixture, only the profile of acetylene is significantly affected by the presence of benzene: the slight consumption by H-abstraction reactions below 1500 K is followed by an increase up to 1700 K due to the fragmentation of the ring.

Concerning the single-ring aromatic products, the presence of acetylene in the initial mixture or as a product of the thermal decomposition of ethylene or the C_3 fuels results, at different extents, in the formation of large mole fractions of phenylacetylene compared to the pure benzene case through the C_6H_5+C_2H_2 reaction. Phenylacetylene has a central role in the formation of large PAHs. For similar reasons, the concentrations of diethynyl benzene are higher in the binary mixtures compared to the benzene case. Styrene is one of the main products in the benzene + ethylene and benzene + propylene case, through the reactions C_6H_5+C_2H_4 and C_6H_6+C_2H_3, while it is produced in smaller amounts in the benzene + propyne co-pyrolysis. The presence of the C_3 fuels also promotes the formation of toluene and other alkylated aromatic hydrocarbons.

The chemistry of the PAH products is strongly affected by the reactions involving the added unsaturated hydrocarbons. In particular, the central role of the reactions involving C_3 intermediates and the single ring in the formation of indene has been experimentally confirmed and validated for the first time. In the benzene + C_3 co-pyrolysis, the indenyl radical is also important for the formation of methyl indene and benzofulvene, which are fundamental precursors of naphthalene, and acenaphthylene. These pathways complement the conventional HACA routes. Indeed, naphthalene and acenaphthylene formation is highly enhanced when C_3 fuels are considered compared to benzene + ethylene co-pyrolysis and benzene + acetylene co-pyrolysis. In the benzene + C_2 cases, the HACA routes are the main sources of naphthalene although the low H-atom concentrations inhibits the $C_{10}H_7$ + H reaction. Regarding acenaphthylene, in the benzene + acetylene co-pyrolysis the HACA route and the thermal decomposition / isomerization of biphenyl play a major role, while for benzene + ethylene co-pyrolysis, an additional route through the reaction $C_{10}H_7$ + C_2H_4 is accessible. The abundance of C_2H_2 in the reaction system of the binary fuels results in numerous compounds with ethynyl branches such as ethynyl naphthalene, diethynyl naphthalene, ethynyl acenaphthylene, and ethynyl biphenyl. On the other hand, the reactions of $C_{10}H_7$ radicals with CH_3 and C_3 species in benzene-C_3 co-pyrolysis lead to the formation of methyl naphthalene and enhance the production of fluorene, respectively. Finally, the formation pathways to the C_{14} products are similar for all cases, although significantly enhanced by the presence higher phenylacetylene concentrations in the cases of binary mixtures.

Declaration of Competing Interest

The authors declare that they have no known competing financial interests or personal relationships that could have appeared to influence the work reported in this paper.

Acknowledgement

This project has received funding from the European Research Council (ERC) under the European Union's Horizon 2020 research and innovation program (grant agreement n° 756785).

Supplementary materials

Supplementary material associated with this article can be found, in the online version, at doi:10.1016/j.combustflame.2021.111858.

References

[1] H. Wang, Formation of nascent soot and other condensed-phase materials in flames, Proc. Combust. Inst. 33 (2011) 41–67.
[2] D.K. Verma, K.d. Tombe, Benzene in gasoline and crude oil: occupational and environmental implications, AIHA J. 63 (2002) 225–230.
[3] H.R. Zhang, E.G. Eddings, A.F. Sarofim, Criteria for selection of components for surrogates of natural gas and transportation fuels, Proc. Combust. Inst. 31 (2007) 401–409.
[4] H. Richter, J.B. Howard, Formation of polycyclic aromatic hydrocarbons and their growth to soot—A review of chemical reaction pathways, Prog. Energy Combust. Sci. 26 (2000) 565–608.
[5] H. Richter, T.G. Benish, O.A. Mazyar, W.H. Green, J.B. Howard, Formation of polycyclic aromatic hydrocarbons and their radicals in a nearly sooting premixed benzene flame, Proc. Combust. Inst. 28 (2000) 2609–2618.
[6] K.C. Hou, H.B. Palmer, The kinetics of thermal decomposition of benzene in a flow system, J. Phys. Chem. 69 (1965) 863–868.
[7] R.D. Kern, H.J. Singh, M.A. Esslinger, P.W. Winkeler, Product profiles observed during the pyrolyses of toluene, benzene, butadiene, and acetylene, Symp. (Int.) Combust. 19 (1982) 1351–1358.
[8] A. Laskin, A. Lifshit, Thermal decomposition of benzene. Single-pulse shock–tube investigation, Symp. (Int.) Combust. 26 (1996) 669–675.
[9] R. Sivaramakrishnan, K. Brezinsky, R. Tranter, A shock-tube study of the high–pressure thermal decomposition of benzene, Combust. Sci. Technol. 178 (2006) 285–305.
[10] R.S. Tranter, S.J. Klippenstein, L.B. Harding, B.R. Giri, X. Yang, J.H. Kiefer, Experimental and theoretical investigation of the self-reaction of phenyl radicals, J. Phys. Chem. A 114 (2010) 8240–8261.
[11] H. Böhm, H. Jander, D. Tanke, PAH growth and soot formation in the pyrolysis of acetylene and benzene at high temperatures and pressures: modeling and experiment, Symp. (Int.) Combust. 27 (1998) 1605–1612.
[12] B. Shukla, M. Koshi, A highly efficient growth mechanism of polycyclic aromatic hydrocarbons, Phys. Chem. Chem. Phys. 12 (2010) 2427–2437.
[13] A. Comandini, T. Malewicki, K. Brezinsky, Chemistry of polycyclic aromatic hydrocarbons formation from phenyl radical pyrolysis and reaction of phenyl and acetylene, J. Phys. Chem. A 116 (2012) 2409–2434.
[14] C. Saggese, A. Frassoldati, A. Cuoci, T. Faravelli, E. Ranzi, A wide range kinetic modeling study of pyrolysis and oxidation of benzene, Combust. Flame 160 (2013) 1168–1190.
[15] W. Sun, A. Hamadi, S. Abid, N. Chaumeix, A. Comandini, Probing PAH formation chemical kinetics from benzene and toluene pyrolysis in a single-pulse shock tube, Proc. Combust. Inst. 38 (2021) 891–900.
[16] E. Heckmann, H. Hippler, J. Troe, High-temperature reactions and thermodynamic properties of phenyl radicals, Symp. (Int.) Combust. 26 (1996) 543–550.
[17] M. Braun-Unkhoff, P. Frank, T. Just, A shock tube study on the thermal decomposition of toluene and of the phenyl radical at high temperatures, Symp. (Int.) Combust. 22 (1989) 1053–1061.
[18] C. Horn, P. Frank, R.S. Tranter, J. Schaugg, H.-.H. Grotheer, T. Just, Direct measurement of the reaction pair C6H5NO→C6H5+NO by a combined shock tube and flow reactor approach, Symp. (Int.) Combust. 26 (1996) 575–582.
[19] C. Xu, M. Braun-Unkhoff, C. Naumann, P. Frank, A shock tube investigation of H atom production from the thermal dissociation of ortho-benzyne radicals, Proc. Combust. Inst. 31 (2007) 231–239.
[20] H. Wang, M. Frenklach, Calculations of rate coefficients for the chemically activated reactions of acetylene with vinylic and aromatic radicals, J. Phys. Chem. 98 (1994) 11465–11489.
[21] I.V. Tokmakov, M.C. Lin, Reaction of phenyl radicals with acetylene: quantum chemical investigation of the mechanism and master equation analysis of the kinetics, J. Am. Chem. Soc. 125 (2003) 11397–11408.
[22] A.M. Mebel, Y. Georgievskii, A.W. Jasper, S.J. Klippenstein, Temperature- and pressure-dependent rate coefficients for the HACA pathways from benzene to naphthalene, Proc. Combust. Inst. 36 (2017) 919–926.
[23] A. Fahr, S.E. Stein, Reactions of vinyl and phenyl radicals with ethyne, ethene and benzene, Symp. (Int.) Combust. 22 (1989) 1023–1029.
[24] I.V. Tokmakov, M.C. Lin, Combined quantum chemical/RRKM-ME computational study of the phenyl + ethylene, vinyl + benzene, and H + styrene reactions, J. Phys. Chem. A 108 (2004) 9697–9714.
[25] T.-.C. Chu, Z.J. Buras, B. Eyob, M.C. Smith, M. Liu, W.H. Green, Direct kinetics and product measurement of phenyl radical + ethylene, J. Phys. Chem. A 124 (2020) 2352–2365.
[26] T. Yu, M.C. Lin, Kinetics of the phenyl radical reaction with ethylene: an RRKM theoretical analysis of low and high temperature data, Combust. Flame 100 (1995) 169–176.
[27] V.V. Kislov, A.M. Mebel, Ab initio G3-type/statistical theory study of the formation of indene in combustion flames. I. Pathways involving benzene and phenyl radical, J. Phys. Chem. A 111 (2007) 3922–3931.

[28] A.M. Mebel, Y. Georgievskii, A.W. Jasper, S.J. Klippenstein, Pressure-dependent rate constants for PAH growth: formation of indene and its conversion to naphthalene, Faraday Discuss 195 (2017) 637–670.
[29] L. Vereecken, J. Peeters, H.F. Bettinger, R.I. Kaiser, P.v.R. Schleyer, H.F. Schaefer, Reaction of phenyl radicals with propyne, J. Am. Chem. Soc. 124 (2002) 2781–2789.
[30] L. Vereecken, J. Peeters, Reactions of chemically activated C9H9 species II: the reaction of phenyl radicals with allene and cyclopropene, and of benzyl radicals with acetylene, Phys. Chem. Chem. Phys. 5 (2003) 2807–2817.
[31] L. Vereecken, H.F. Bettinger, J. Peeters, Reactions of chemically activated C9H9 species, Phys. Chem. Chem.Phys. 4 (2002) 2019–2027.
[32] A.N. Morozov, A.M. Mebel, Theoretical study of the reaction mechanism and kinetics of the phenyl + allyl and related benzyl + vinyl associations, J. Phys. Chem. A, Molecules, Spectroscopy, Kinetics, Environment, and General Theory 123 (2019).
[33] A.N. Morozov, A.M. Mebel, Theoretical study of the reaction mechanism and kinetics of the phenyl + propargyl association, Phys. chem. chem. phys. : PCCP 22 (2020) 6868–6880.
[34] M. Frenklach, H. Wang, Detailed modeling of soot particle nucleation and growth, Symp. (Int.) Combust. 23 (1991) 1559–1566.
[35] J. Appel, H. Bockhorn, M. Frenklach, Kinetic modeling of soot formation with detailed chemistry and physics: laminar premixed flames of C2 hydrocarbons, Combust. Flame 121 (2000) 122–136.
[36] B. Shukla, M. Koshi, A novel route for PAH growth in HACA based mechanisms, Combust. Flame 159 (2012) 3589–3596.
[37] W. Sun, A. Hamadi, S. Abid, N. Chaumeix, A. Comandini, An experimental and kinetic modeling study of phenylacetylene decomposition and the reactions with acetylene/ethylene under shock tube pyrolysis conditions, Combust. Flame 220 (2020) 257–271.
[38] W. Sun, A. Hamadi, S. Abid, N. Chaumeix, A. Comandini, Detailed experimental and kinetic modeling study of toluene/C2 pyrolysis in a single-pulse shock tube, Combust. Flame 226 (2021) 129–142.
[39] W. Sun, A. Hamadi, S. Abid, N. Chaumeix, A. Comandini, A comparative kinetic study of C8–C10 linear alkylbenzenes pyrolysis in a single-pulse shock tube, Combust. Flame 221 (2020) 136–149.
[40] W. Sun, A. Hamadi, S. Abid, N. Chaumeix, A. Comandini, A comprehensive kinetic study on the speciation from propylene and propyne pyrolysis in a single-pulse shock tube, Combust. Flame 231 (2021) 111485.
[41] W.J.M. Rankine, XV. On the thermodynamic theory of waves of finite longitudinal disturbance, Philos. Trans. R. Soc. London 160 (1870) 277–288.
[42] P.H. Hugoniot, Sur la Propagation du Mouvement dans les Corps et Spécialement dans les Gaz Parfaits (première partie), 57 (1887) 3–97.
[43] P.H. Hugoniot, Sur la Propagation du Mouvement dans les Corps et Spécialement dans les Gaz Parfaits (deuxième partie), 58 (1889) 1–125.
[44] X. Han, J.M. Mehta, K. Brezinsky, Temperature approximations in chemical kinetics studies using single pulse shock tubes, Combust. Flame 209 (2019) 1–12.
[45] P.T. Lynch, C.J. Annesley, C.J. Aul, X. Yang, R.S. Tranter, Recombination of allyl radicals in the high temperature fall-off regime, J. Phys. Chem. A 117 (2013) 4750–4761.
[46] J.A. Manion, D.A. Sheen, I.A. Awan, Evaluated kinetics of the reactions of H and CH_3 with n-alkanes: experiments with n-butane and a combustion model reaction network analysis, J. Phys. Chem. A 119 (2015) 7637–7658.
[47] W. Tang, K. Brezinsky, Chemical kinetic simulations behind reflected shock waves, Int. J. Chem. Kinet. 38 (2006) 75–97.
[48] A. Comandini, T. Malewicki, K. Brezinsky, Online and offline experimental techniques for polycyclic aromatic hydrocarbons recovery and measurement, Rev. Sci. Instrum. 83 (2012) 034101.
[49] W. Pejpichestakul, E. Ranzi, M. Pelucchi, A. Frassoldati, A. Cuoci, A. Parente, T. Faravelli, Examination of a soot model in premixed laminar flames at fuel-rich conditions, Proc. Combust. Inst. 37 (2019) 1013–1021.
[50] P. Liu, Z. Li, A. Bennett, H. Lin, S.M. Sarathy, W.L. Roberts, The site effect on PAHs formation in HACA-based mass growth process, Combust. Flame 199 (2019) 54–68.
[51] L.B. Tuli, A.M. Mebel, Formation of phenanthrene via H-assisted isomerization of 2-ethynylbiphenyl produced in the reaction of phenyl with phenylacetylene, Int. J. Chem. Kinet. 52 (2020) 875–883.
[52] T.-C. Chu, M.C. Smith, J. Yang, M. Liu, W.H. Green, Theoretical study on the HACA chemistry of naphthalenyl radicals and acetylene: the formation of C12H8, C14H8, and C14H10 species, Int. J. Chem. Kinet. 52 (2020) 752–768.
[53] L. Zhao, M. Prendergast, R.I. Kaiser, B. Xu, U. Ablikim, W. Lu, M. Ahmed, A.D. Oleinikov, V.N. Azyazov, A.H. Howlader, S.F. Wnuk, A.M. Mebel, How to add a five-membered ring to polycyclic aromatic hydrocarbons (PAHs) - molecular mass growth of the 2-naphthyl radical (C(10)H(7)) to benzindenes (C(13)H(10)) as a case study, Phys. chem. chem. phys. : PCCP 21 (2019) 16737–16750.
[54] A. Oleinikov, A. Mebel, V. Azyazov, Kinetics of Reactions of 1- and 2–Naphthyl with Propyne and Allene, B. Lebedev Phys. INST+. 47 (2020) 97–100.
[55] E.R. Ritter, J.W. Bozzelli, THERM: thermodynamic property estimation for gas phase radicals and molecules, Int. J. Chem. Kinet. 23 (1991) 767–778.
[56] COSILABThe Combustion Simulation Laboratory, Rotexo GmbH & Co., KG, Haan, Germany, 2009 Version 3.3.2.
[57] L.A. Mertens, I.A. Awan, D.A. Sheen, J.A. Manion, Evaluated site-specific rate constants for reaction of isobutane with H and CH3: shock tube experiments combined with bayesian model optimization, J. Phys. Chem. A 122 (2018) 9518–9541.
[58] A. Comandini, K. Brezinsky, Theoretical study of the formation of naphthalene from the radical/π-bond addition between single-ring aromatic hydrocarbons, J. Phys. Chem. A 115 (2011) 5547–5559.
[59] H. Jin, L. Xing, J. Hao, J. Yang, Y. Zhang, C. Cao, Y. Pan, A. Farooq, A chemical kinetic modeling study of indene pyrolysis, Combust. Flame 206 (2019) 1–20.
[60] A. Comandini, S. Abid, N. Chaumeix, Polycyclic Aromatic Hydrocarbon Growth by Diradical Cycloaddition/Fragmentation, J. Phys. Chem. A 121 (2017) 5921–5931.